Dynamic prediction of displacement and deformation of any point on mining surface based on B-normal model

Xinming Ding[1,2] · Keming Yang[1] ⬤ · Cheng Zhang[3] · Shuang Wang[1] · Zhixian Hou[1] · Hengqian Zhao[1]

Abstract

The surface displacement and deformation of goaf caused by coal mining destroy the underground rock structure and surface ecological environment in the mining area and endanger the safety of human life and property. An accurate and efficient dynamic prediction system of mining subsidence is indispensable. Given the limited scope of the application of the probability integral model on the edge of the mobile basin, its poor prediction effect, and its low accuracy, a new mining subsidence prediction model based on the Boltzmann function is proposed. Combined with the transformed normal distribution time function, a B-normal prediction model that can predict the dynamic displacement and deformation of any point on the surface was constructed. The global optimal solution of the parameters of the dynamic prediction model was inversed by introducing particle swarm optimization shuffled frog leaping intelligent algorithm (PSO-SFLA), and then, the model was applied to the 8102 working face of the Guobei coal mine to dynamically predict the subsidence, inclination, curvature, horizontal displacement, and horizontal deformation of the goaf surface. The prediction results showed that on the strike and dip observation lines, the prediction accuracy of the dynamic subsidence and horizontal displacement of the surface could reach the centimeter level, the predicted root mean square error (RMSE) of dynamic tilt and horizontal deformation was less than 0.51 mm/m, and the predicted RMSE of dynamic curvature was within 0.020 mm/m^2. The prediction results reflected the dynamic evolution law of surface displacement and deformation and verified the reliability of the B-normal dynamic prediction model, which can fully meet the needs of practical engineering applications.

Keywords Mining subsidence · Boltzmann function model · Normal distribution time function · PSO-SFLA algorithm · Dynamic displacement deformation · Dynamic prediction

Introduction

The mining of underground coal resources destroys the rock mass structure in the goaf, causing the displacement and deformation of the rock stratum and the surface. This results in various types of mining damage to the surface within the

✉ Keming Yang
  ykm69@163.com

1 School of Earth Science and Mapping Engineering,
   China University of Mining and Technology (Beijing),
   Beijing 100083, China

2 TBEA Group International Engineering Co., Ltd, Tianjin
   Electric Power Design Institute Co., Ltd, Tianjin 301700, China

3 Communication and Defense Geological Survey Department
   of Huaibei Mining Co., Ltd, Huaibei 235000, Anhui, China

mining-affected area, such as the destruction of buildings (structures), landslides, ground cracks, subsidence, and ponding, which seriously threaten the safety of the properties in the mining area and the lives of the surrounding residents, affecting their normal productivity and lifestyle (Chi et al. 2021a; Wang et al. 2021a Li et al. 2020; Liu et al. 2019). Therefore, it is very important to study the complex spatiotemporal movement process and displacement deformation mechanism of mining subsidence and establish an effective monitoring and prediction system to guide the mining of coal resources and the management of the ecological environment in mining areas.

The existing surface subsidence prediction models can be divided into three categories: the first comprises empirical methods based on measured data, such as the profile function method, typical curve method, and Weibull distribution method (Zuo et al. 2017). The second type is the influence function method. Among the many influence functions, the most commonly used is the probability integration method

(PIM). The third comprises simulation research methods, such as the numerical simulation method, theoretical model method, and similar material simulation method (Chang et al. 2015; Unlu et al. 2013; Li et al. 2019a). At present, the prediction model for surface static subsidence is relatively mature, but it cannot meet the needs of practical engineering applications, because it does not reflect the complex process of surface changes across time and space (Hu et al. 2022a). The construction of a dynamic subsidence prediction model has always been a research hotspot and difficulty. Through studying the literature at home and abroad, we found that the combination of a time function and a surface static prediction model is the current mainstream modeling method, which also means that the time function and static prediction model are the key factors affecting the accuracy of the dynamic prediction model.

The time functions commonly used in dynamic prediction models include the Knothe time function (Cui et al. 1999; Hu et al. 2015), Sroka-Schober time function (Gonzalez et al. 2007), normal distribution time function (Zhang et al. 2016), arctangent time function (Nie et al. 2014), Usher time function (Wang et al. 2021b), Weibull time function (Wang et al. 2016), Bertalanffy time function (Gao et al. 2020), logistic time function (Shi et al. 2021), and Gompertz time function (Wang et al. 2022). Cui et al. (1999) pointed out the shortcomings of the Knothe time function after an in-depth study and provided a determination method for the time coefficient. Zhang et al. (2020) proposed a segmented Knothe time function based on the probability integral model and built a prediction model for any point on the surface given the shortcomings of the Knothe time function. On this basis, Hu et al. proposed a new parameter calculation method of time function based on the normalization method and the least square principle, which can be used for effective land acquisition surface settlement, settlement velocity, and acceleration of mining areas (Hu et al. 2022b). Wang et al. (2021a) introduced the Usher function, which predicts information growth, into their prediction model for dynamic surface subsidence and predicted the settlement at any point on the strike and dip in the main section. Wang et al. (2022) proposed a Gompertz time function model suitable for the longwall coal mining process based on the "three original consistency" modeling idea. Through comparison with the measured data, it was proven that the model was consistent with the characteristics of surface point subsidence. Li et al. (2016) constructed a dynamic prediction model for any point and at any time on the surface based on the normal distribution function and the prediction formula for surface subsidence and used the spatial fitting method to obtain the model parameters, which confirmed the spatio-temporal completeness of the normal distribution time function. Zhang et al. (2019a) determined the theoretical defects of the normal distribution time function through comparative analysis

and improved it by using the overall deviation correction method, which overcomes the limitations of time parameter selection and widens the application range of the normal distribution time function.

Through the literature analysis, it could be seen that the above model combines the commonly used probability integral depression prediction method in the application process. Although this method fits the central area of the subsidence basin well, due to the relatively fast convergence speed, the fitting accuracy of the edge of the subsidence basin is not particularly ideal, which limits its popularization and application. The Boltzmann function prediction model not only has high accuracy for the center of the subsidence basin but also converges relatively slowly at the edge of the basin. This model is more practical than the PIM model and has a wide range of adaptability. Considering that most of the current studies are only limited to the monitoring and prediction of dynamic subsidence, there are few relevant studies on other moving deformation indicators. Therefore, based on the Boltzmann function model (Zhang et al. 2021; Wang et al. 2013; Li et al. 2021; Chi et al. 2021b), combined with the transformed normal distribution time function with space-time completeness, we built a dynamic prediction model (B-normal model) for the displacement and deformation of any point on the surface under the influence of mining. The particle swarm optimization shuffled frog leaping algorithm was used to inverse the model parameters, and the dynamic prediction of subsidence (W), inclination (I), curvature (K), horizontal displacement (U), and horizontal deformation (ε) at any time at any point on the surface of the goaf was carried out to overcome the limitations of the PIM model to a certain extent and improve the prediction accuracy, providing concrete reference for the environmental geological disaster warning and mining damage identification in the mining area.

Models and methods

Boltzmann function prediction model

Boltzmann extended Maxwell distribution to Maxwell-Boltzmann distribution (Adhelacahya et al. 2020). This research result has been widely used in mining subsidence prediction, bearing capacity prediction, mineral target prediction, atmospheric dynamics model construction, and other fields (Liu et al. 2011; Chen et al. 2012; Liu et al. 2003). The expression of the Boltzmann function is $y = \frac{A_1 - A_2}{1 + e^{(x - x_0)/b}} + A_2$; it is not difficult to find that the shape of this function curve is a typical anti-"S" curve, which is similar to the subsidence curve of the main section of the surface moving basin during semi-infinite mining. Its subsidence prediction formula is

$$W(x) = \frac{W_0}{2}\left[\text{erf}\left(\frac{\sqrt{\pi}}{r}x\right) + 1\right] \tag{1}$$

where W_0 is the final surface subsidence, r is the main influence radius, and x is the position of the point on the main section.

Combining the form of the Boltzmann function and formula (1), the subsidence prediction formula for the main section of the surface displacement basin during semi-infinite mining can be preliminarily defined as (Wang et al. 2013)

$$W(x) = k\frac{W_0}{1 + \exp\left(-(x-s)/R\right)} \tag{2}$$

where k is the scale factor, s is the offset of the inflection point of the working face, and R is the new main influence radius related to r.

After data fitting and analysis of Eq. (2) with MATLAB software, the scale coefficient $k = 1$ can be determined, and the final form of Eq. (2) is

$$W(x) = \frac{W_0}{1 + \exp\left(-(x-s)/R\right)} \tag{3}$$

It is easy to know that when $x \to \infty$, there are $\exp(-(x-s)/R) \to 0$, and then, $W(x) \to W_0$. When $x = s$, there are $W(x) = \frac{W_0}{2}$. At this time, the subsidence at the inflection point of the subsidence curve is half of the maximum subsidence, which conforms to the general law of mining subsidence. To further verify the correctness of the Boltzmann function, numerical model experiments were carried out in the MATLAB software to predict the subsidence between -500 and 500 m from the open cut of the working face. The comparison results between the Boltzmann function prediction model and the PIM prediction model are shown in Fig. 1. It can be seen from Fig. 1 that the two function curves were consistent. The main difference was that the convergence speed of the Boltzmann function curve at the edge of the subsidence basin was slower than that of the PIM curve, which was more in line with the dynamic characteristics of ground points in the goaf. In addition, by referring to the research of Zhang et al. (2021), the two prediction models can share a set of parameter systems $P = [q, b, \theta_0, \tan\beta, S_1, S_2, S_3, S_4]$ after some numerical conversion of the predicted parameters, which also greatly improves the efficiency of parameter inversion.

The element influence function of the Boltzmann function prediction model can be obtained by differentiating Eq. (2) as (Chi et al. 2021a)

$$w_e(x) = dW(x) = \frac{1}{R}\frac{\exp\left(-x/R\right)}{(1 + \exp\left(-x/R\right))^2} \tag{4}$$
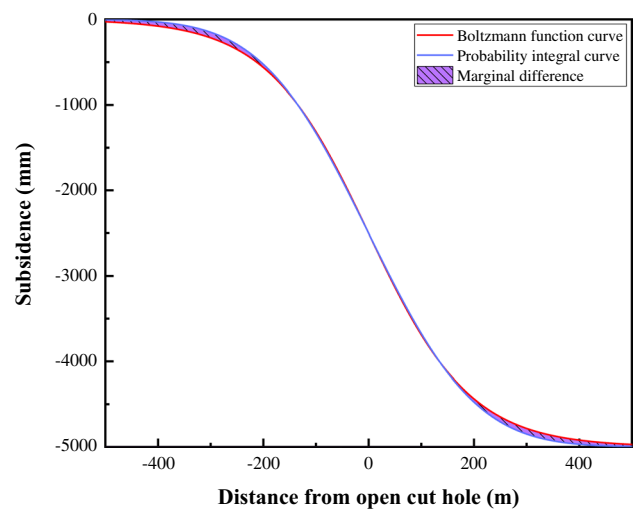

Fig. 1 Comparison of subsidence curves of Boltzmann and PIM predicted models during semi-infinite mining

According to the derivation experience of the probability integral method and the knowledge of elasticity, the horizontal displacement function of the element can be determined as

$$U_e(x) = B\frac{dw_e(x)}{dx} \tag{5}$$

In the formula, B is a constant. By integrating formula (5), the horizontal displacement prediction formula of any point on the surface of semi-infinite mining along the x direction can be obtained as

$$U(x) = W_0\frac{B}{R}\frac{\exp\left(-x/R\right)}{(1 + \exp\left(-x/R\right))^2} \tag{6}$$

Let $b' = \frac{B}{R}$; then, the above formula can be simplified as

$$U(x) = b'W_0\frac{\exp\left(-x/R\right)}{(1 + \exp\left(-x/R\right))^2} \tag{7}$$

where b' is the new horizontal displacement coefficient.

Surface subsidence curve formula of semi-infinite and limited mining on the main section of the trend modeled by the PIM prediction model is as follows:

$$\begin{cases} W^0(x) = \frac{W_0}{2}\left[\text{erf}\left(\frac{\sqrt{\pi}}{r}x\right) + 1\right] \\ W(x) = W^0(x) - W^0(x - l) \end{cases} \tag{8}$$

where $W_0 = mq\cos\alpha$, m is the mining thickness of the working face, q is the subsidence coefficient, α is the dip angle of the working face, and l is the calculated length of the working face strike. According to the coordinate system of the main section of the surface strike during limited mining
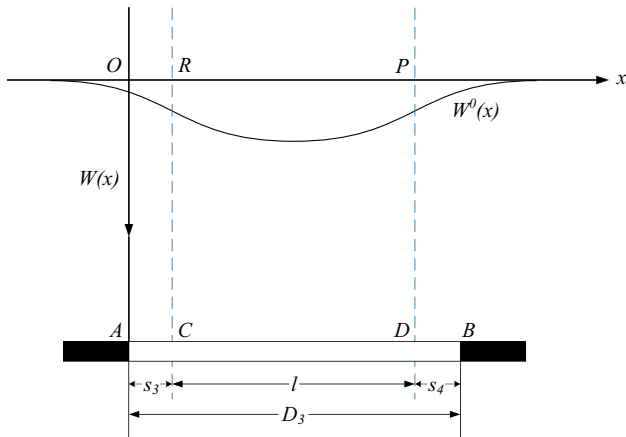
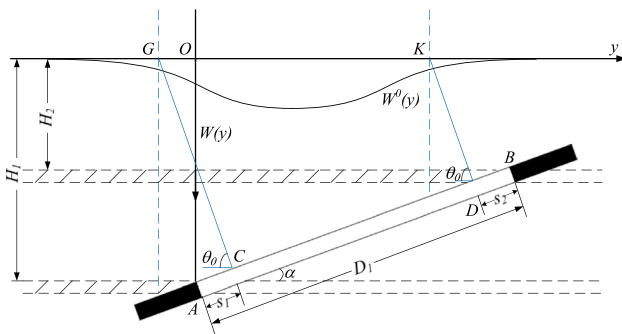**Fig. 2** Main cross-section coordinate system along strike

Fig. 3 Main cross-section coordinate system along dip

as shown in Fig. 2, the prediction formula of the Boltzmann function prediction model on the main section of the surface movement basin strike during limited mining can be deduced as follows:

$$W^0(x) = w(x) - w(x-l) = mq\cos\alpha \left(\frac{1}{1+\exp\left(-\frac{x-s_3}{R}\right)} - \frac{1}{1+\exp\left(-\frac{x-D_3+s_3+s_4}{R}\right)} \right)$$ (9)

where D_3 is the strike length of the working face and s_3 and s_4 are the offset of the left and right turning points of the working face, respectively.

The coordinate system of the main section of the surface dip during the limited mining of the working face is shown in Fig. 3. According to the equal influence principle, the Boltzmann function prediction model can be derived. The subsidence prediction formula on the main section of the dip of the surface movement basin during the limited mining is

$$\begin{cases} w(y) = \dfrac{mq\cos\alpha}{1+\exp(-\frac{y+(H_1-s_1\sin\alpha)\cot\theta_0-s_1\cos\alpha}{R_1})} \\ w(y-L) = \dfrac{mq\cos\alpha}{1+\exp(-\frac{y+(H_1-s_1\sin\alpha)\cot\theta_0-s_1\cos\alpha-(D_1-s_1-s_2)\frac{\sin(\theta_0+\alpha)}{\sin\theta_0}}{R_1})} \\ W^0(y) = w(y) - w(y-L) \end{cases}$$ (10)

where θ_0 is the propagation angle of mining influence; s_1 and s_2 are the offset of lower and upper inflection points of the working face, respectively; D_1 is the inclined length of the working face; H_1 is the downhill mining depth of the working face; and R_1 and R_2 are the new main influence radii related to r.

From the above analysis, it can be seen that the main section subsidence prediction formula of semi-infinite mining trend is (Jiang et al. 2021)

$$W(x) = \frac{W_0}{1+\exp(-x/R)}$$ (11)

The surface inclination $i(x)$ along the x direction is the first derivative of subsidence to x, that is,

$$i(x) = \frac{dW(x)}{dx} = \frac{W_0}{R}\frac{\exp(-x/R)}{(1+\exp(-x/R))^2}$$ (12)

The surface inclination $K(x)$ along the x direction is the second derivative of subsidence to x, that is,

$$K(x) = \frac{d^2W(x)}{dx^2} = -\frac{W_0}{R^2}\frac{\exp(-x/R)(1-\exp(-x/R))}{(1+\exp(-x/R))^3}$$ (13)

From Eqs. (7) and (12), the relationship between horizontal displacement and inclination is

$$U(x) = b'Ri(x)$$ (14)

For the new main influence radius R, Wang et al. (2013) found that the ratio of R to the main influence radius r approaches a constant through several examples and obtained $R \approx r/4.13$. According to the definition $b = \frac{B}{r}$ of horizontal displacement coefficient, Eq. (14) can be transformed into

$$U(x) = b'Ri(x) = 4.13Rbi(x)$$ (15)

The horizontal deformation $\varepsilon(x)$ of the surface along the x direction is defined as the first derivative of the horizontal displacement $U(x)$ to x, that is,

$$\varepsilon(x) = \frac{dU(x)}{dx} = 4.13bR\frac{di(x)}{dx} = 4.13bRK(x)$$ (16)

Substitute Eq. (13) into the above equation to obtain

$$\varepsilon(x) = -4.13b\frac{W_0}{R}\frac{\exp\left(-\frac{x}{R}\right)\left(1-\exp\left(-\frac{x}{R}\right)\right)}{(1+\exp(-x/R))^3} \tag{17}$$

To sum up, when the dip is fully mined, the calculation formula for the displacement and deformation value of the main section of the limited mining trend is

$$\begin{cases} W^0(x) = W(x) - W(x-l) \\ i^0(x) = i(x) - i(x-l) \\ K^0(x) = K(x) - K(x-l) \\ U^0(x) = U(x) - U(x-l) \\ \varepsilon^0(x) = \varepsilon(x) - \varepsilon(x-l) \end{cases} \tag{18}$$

Similarly, when the strike is fully mined, the calculation formula for the displacement and deformation value of the main section of the limited mining tendency is

$$\begin{cases} W^0(y) = W(y) - W(y-L) \\ i^0(y) = i(y) - i(y-L) \\ K^0(y) = K(y) - K(y-L) \\ U^0(y) = U(y) - U(y-L) + W^0(y)\cot\theta_0 \\ \varepsilon^0(y) = \varepsilon(y) - \varepsilon(y-L) + i^0(y)\cot\theta_0 \end{cases} \tag{19}$$

where $W^0(y)\cot\theta_0$ and $i^0(y)\cot\theta_0$ are the horizontal displacement and horizontal deformation components caused by coal seam inclination, respectively.

According to the main section coordinate system of strike and dip shown in Fig. 2 and Fig. 3, the final subsidence $W(x,y)$ at any point on the surface of the gob mobile basin can be expressed as

$$W(x,y) = \frac{W^0(x)W^0(y)}{W_0} \tag{20}$$

In the formula, $W^0(x)$ is the subsidence function of any point on the strike main section when the strike is fully mined, and $W^0(y)$ is the subsidence function of any point on the strike main section when the strike is fully mined, which is calculated according to formula (18) and formula (19), respectively.

The inclination value $i(x,y,\varphi)$ of any point (x,y) on the surface along the direction φ (the angle from the positive direction of the x-axis to the specified calculation direction) is the directional derivative of the subsidence $W(x,y)$ in the direction φ, which can be expressed as

$$i(x,y,\varphi) = \frac{1}{W_0}\left[i^0(x)W^0(y)\cos\varphi + i^0(y)W^0(x)\sin\varphi\right] \tag{21}$$

The curvature value $K(x,y,\varphi)$ of any point (x,y) on the surface along the direction φ is the directional derivative of inclination $i(x,y,\varphi)$ in the direction φ, which can be expressed as

$$K(x,y,\varphi) = \frac{1}{W_0}\left[K^0(x)W^0(y)\cos^2\varphi + K^0(y)W^0(x)\sin^2\varphi + i^0(x)i^0(y)\sin 2\varphi\right] \tag{22}$$

According to the numerical relationship between horizontal displacement and tilt curve, the horizontal displacement value $U(x,y,\varphi)$ of any point (x,y) on the surface along the φ direction can be expressed as

$$U(x,y,\varphi) = 4.13bRi(x,y,\varphi) \tag{23}$$

According to the numerical relationship between horizontal deformation and curvature curve, the horizontal deformation value $\varepsilon(x,y,\varphi)$ of any point (x,y) on the surface along the direction φ can be expressed as

$$\varepsilon(x,y,\varphi) = 4.13bRK(x,y,\varphi) \tag{24}$$

Normal distribution time function and its parameter determination

Normal distribution time function

Normal distribution, also known as Gaussian distribution, is widely used in statistics, physics, mechanics, engineering, and other fields (Li et al. 2019; Huang et al. 2020). Its mathematical expression is as follows:

$$F(x) = \frac{1}{2\sqrt{\pi}\sigma}\int_{-\infty}^{x} e^{-\frac{(x-\mu)^2}{2\sigma^2}}dx \tag{25}$$

where μ is the mean value and σ is the standard deviation.

The normal distribution time function image is shown in Fig. 4. It can be seen that its curve shape is a typical "S" shape, and the value range of $F(x)$ is [0, 1]. The curve function value increases slowly from 0 in the first segment. After reaching the middle section, it shows a rapidly increasing trend. The latter segment slowly converges to 1 and does not increase after reaching 1. It demonstrated the same characteristics as the surface point subsidence caused by underground mining, so it could be preliminarily judged that the normal distribution function was suitable for the time function of mining subsidence dynamic prediction.

The expressions of subsidence velocity $v(x)$ and subsidence acceleration $a(x)$ can be obtained by calculating the first and second derivatives of the normal distribution time function, as shown in Eqs. (26) and (27), respectively. The function images are shown in Fig. 5a and Fig. 5b.

$$v(x) = F'(x) = \frac{1}{\sqrt{2\pi}\sigma}e^{-\frac{(x-\mu)^2}{2\sigma^2}} \tag{26}$$

$$a(x) = F''(x) = -\frac{1}{\sqrt{2\pi}\sigma^3}(x-\mu)e^{-\frac{(x-\mu)^2}{2\sigma^2}} \tag{27}$$
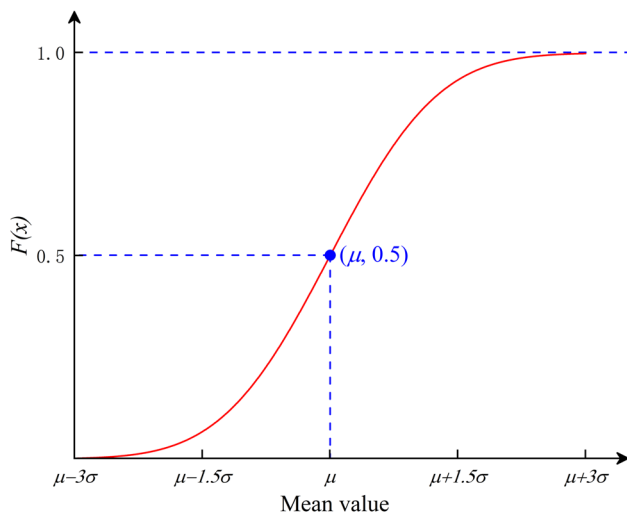
Fig. 4 Normal distribution time function

As can be seen from Fig. 5, the variation trend of subsidence velocity of the normal distribution time function is $0 \rightarrow +v_{\max} \rightarrow 0$. And the variation trend of subsidence acceleration is $0 \rightarrow +a_{\max} \rightarrow 0 \rightarrow -a_{\max} \rightarrow 0$. This fully conforms to the actual dynamic subsidence law caused by mining subsidence, so it can be further determined that the normal distribution time function has good temporal and spatial completeness and is very suitable for the dynamic prediction of surface subsidence.

Parameter analysis of normal distribution time function

According to the general law of mining subsidence, there is a certain time delay in surface subsidence, that is, the time from the beginning of the working face to the occurrence of surface displacement and deformation, expressed in t_s. The surface subsidence progresses through three stages (initial stage, active stage, and declining stage) for with a certain duration. In the

following equations, t_f represents the time from the beginning to the end of surface displacement and deformation. Let

$$\mu = t_s + \frac{t_f}{2} \tag{28}$$

$$t_f = (\mu + \delta\sigma) - (\mu - \delta\sigma) = 2\delta\sigma \Rightarrow \sigma = \frac{t_f}{2\delta} \tag{29}$$

where δ is the shape parameter of subsidence curve, which is related to mining geological conditions.

Substituting μ and σ into Eq. (25) gives

$$F(t) = \frac{2\delta}{\sqrt{2\pi}t_f} \int_{t_s}^{t} e^{-\frac{2\delta^2\left(t - t_s - \frac{t_f}{2}\right)}{t_f^2}} dt \tag{30}$$

The Gaussian error function is introduced to simplify the integral of Eq. (30) (Li et al. 2016).

$$F(t) = \frac{1}{2}\left[\mathrm{erf}\left(\frac{\sqrt{2}\delta}{t_f}\left(t - t_s - \frac{t_f}{2}\right)\right) - \mathrm{erf}\left(-\frac{\sqrt{2}}{2}\delta\right)\right] \tag{31}$$

Equation (31) is the normal distribution time function that can be used for dynamic subsidence of the goaf surface. Assuming that the surface subsidence delay time $t_s = 80$ days and the duration $t_f = 400$ days, when the curve shape parameter $\delta = 1, 2, 3,$ and 4, the function image of Eq. (31) is shown in Fig. 6a. Assuming the curve shape parameter $\delta = 3$, when the surface subsidence delay time $= 30$ days and 80 days, and the duration $t_f = 300$ days and 400 days, the function image of Eq. (31) is shown in Fig. 6b.

It can be seen from Fig. 6a that the parameter δ mainly controls the shape of the curve. Its shape becomes gentle with a decrease in the value of δ, and the final convergence value of the time function also decreases, reflecting the intensity of the displacement and deformation of surface points. It is worth noting that when the morphological parameter $\delta < 2$, the deviation between the final

Fig. 5 Curves of subsidence velocity and acceleration of normal distribution time function. **a** Subsidence velocity. **b** Subsidence acceleration
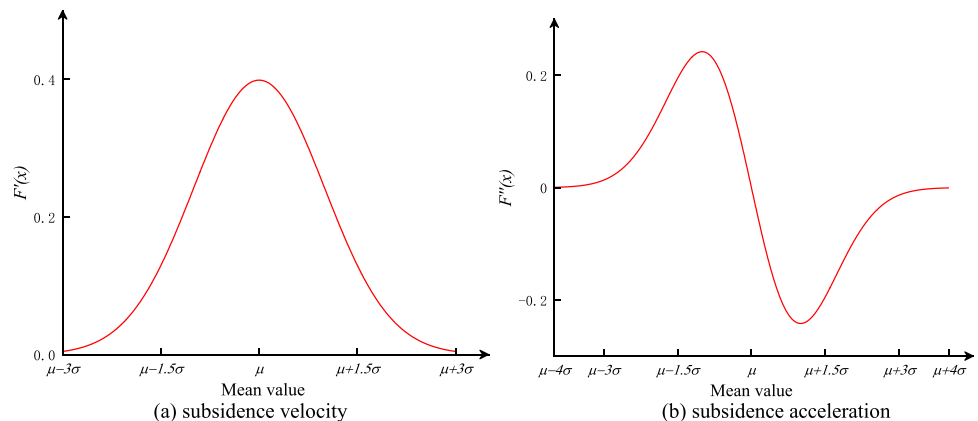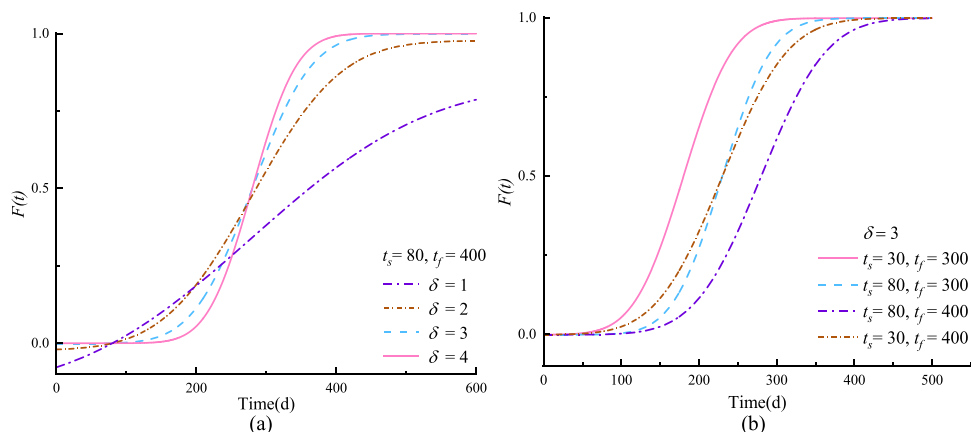

(a) subsidence velocity

(b) subsidence acceleration

Fig. 6 Normal distribution time function image when t_s, t_f, and δ take different values. **a** The change of curve shape when t_s and t_f are fixed and δ takes different values. **b** The change of curve shape when δ is fixed, and t_s and t_f take different values

convergence value of the time function and 1 is too large and does not conform to the characteristic that the value of the time function changes between 0 and 1. In this circumstance, it is not suitable to act as the time function. As can be seen from Fig. 6b, the parameter t_s mainly controls the left-right translation of the curve. Parameter t_f controls the time required for the curve to reach the stable state and reflects the speed of its convergence.

To solve the problem that the value of the morphological parameter δ is constrained, Zhang et al. (2021) improved the original normal distribution time function by using the growth function, so that the value range of parameter δ is no longer limited to more than 2, and the transformed normal distribution time function expression is

$$F(t) = \frac{1}{2}\left[\text{erf}\left(\frac{\sqrt{2}\delta}{t_f}\left(t - t_s - \frac{t_f}{2}\right)\right) + 1\right] - \frac{t_f + 2t_s - 2t}{2t_f}\left[1 + \text{erf}\left(-\frac{\sqrt{2}}{2}\delta\right)\right]$$

(32)

Construction of prediction model for dynamic displacement and deformation of the whole basin and its parameter inversion

Construction of dynamic prediction model

The core idea of the dynamic displacement and the deformation prediction model is as follows: based on the Boltzmann function prediction model proposed in the "Boltzmann function prediction model" section, the displacement and deformation values of any point on the surface can be statically predicted, and the dynamic displacement and deformation of any point on the surface can be determined by introducing the transformed normal distribution time function and multiplying the static prediction results. As shown in Fig. 7, taking dynamic subsidence as an example, in the practice of dynamic

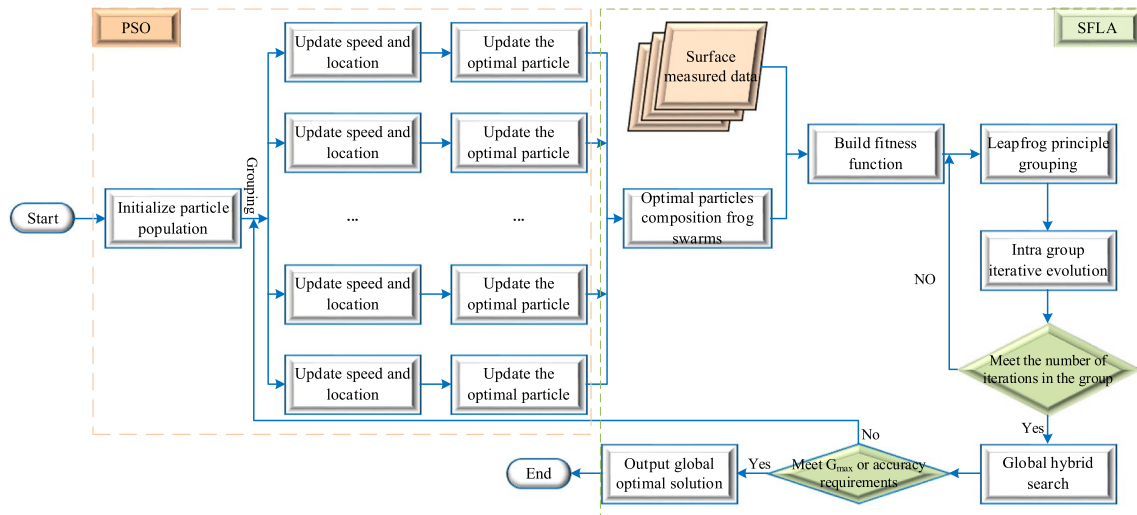**Fig. 7** Dynamic effects of dynamic unit mining on subsidence of surface points
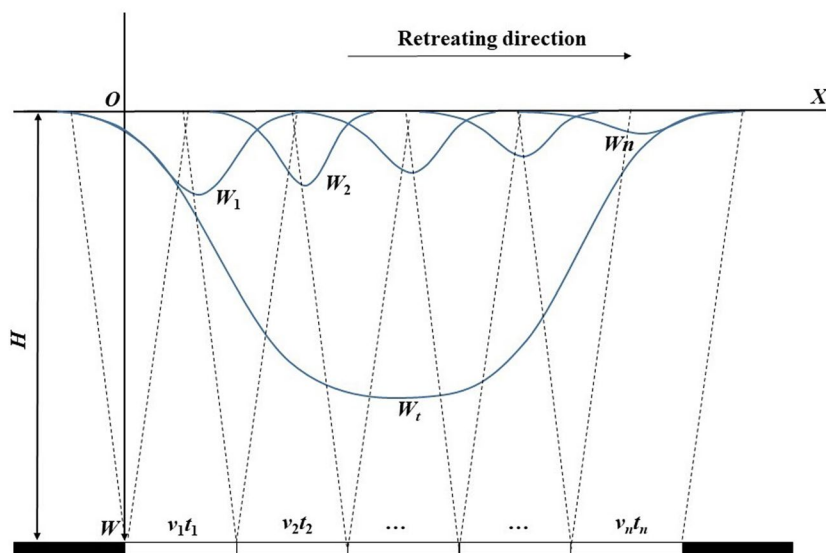
Fig. 8 Technical roadmap for model parameter inversion

prediction, the "effective size segmentation method" is usually used to divide the working face into n independent dynamic mining units, and the mining velocity of each unit is v_1, v_2, ⋯, and v_n, respectively; the mining time of each unit is t_1, t_2, ⋯, and t_n, respectively; the

length of each unit is v_1t_1, v_2t_2, ⋯, and v_nt_n, respectively; W_1, W_2, ⋯, and W_n are the subsidence contributed by each mining unit when the n-th unit is just completed; W_t is the total subsidence; and H is the mining depth. Assuming that the number of mined dynamic units is n
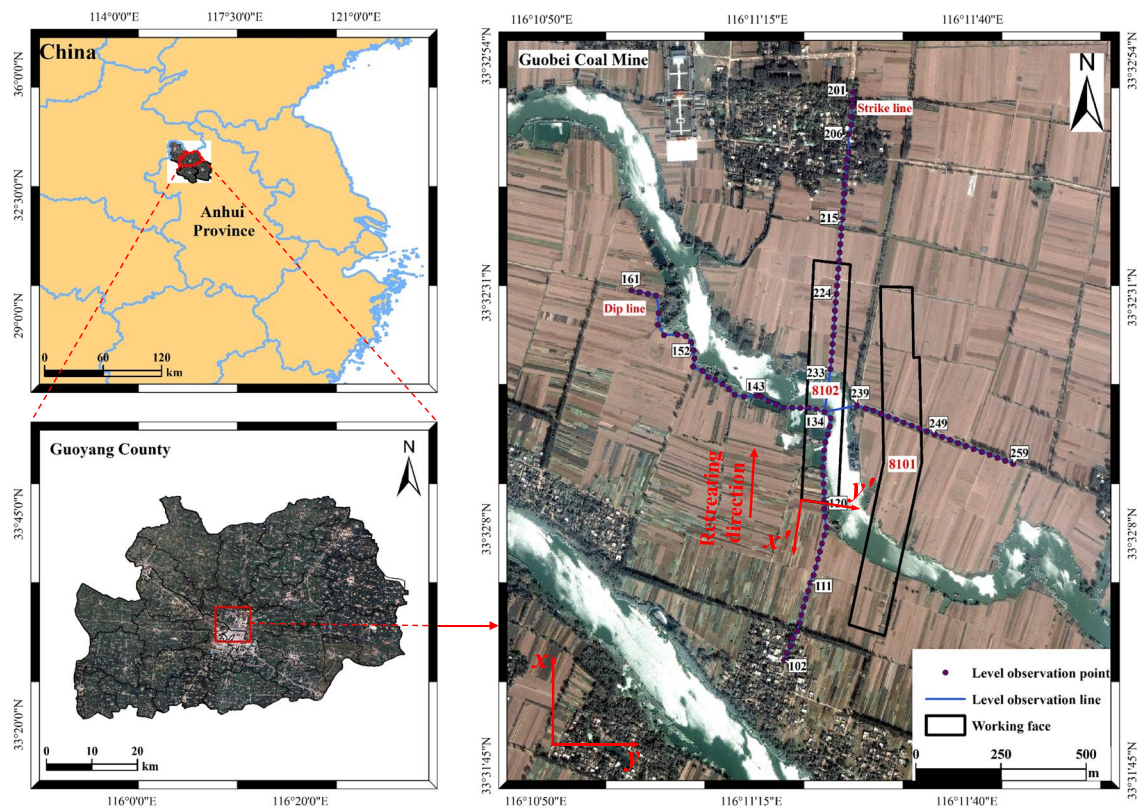

Fig. 9 Position of working face and surface observation line

Table 1 Parameters of 8102 working face in Guobei coal mine

Panel length (m)	Panel width (m)	Mean depth (m)	Mining thickness (m)	Seam dip angle (°)	Start date	Cease date	Mining days (day)	Mean mining velocity (m/day)
724	121	598	7.3	17	2006/12/22	2008/02/25	430	1.7

and the predicted time of surface subsidence is t, the mining time of the first unit is t_1, the mining time of the second unit is $t - t_1$, and the mining time of the n-th unit is $t - \sum_{n=1}^{n-1} t_n$. According to formula (32), the normal distribution time function of each mining unit can be expressed as follows:

1st mining unit:

$$F(t_1) = \frac{1}{2}\left[erf\left(\frac{\sqrt{2}\delta}{t_f}\left(t_1 - t_s - \frac{t_f}{2}\right)\right) + 1\right] - \frac{t_f + 2t_s - 2t_1}{2t_f}\left[1 + erf\left(-\frac{\sqrt{2}}{2}\delta\right)\right]$$

(33)

2nd mining unit:

$$F(t - t_1) = \frac{1}{2}\left[erf\left(\frac{\sqrt{2}\delta}{t_f}\left(t - t_1 - t_s - \frac{t_f}{2}\right)\right) + 1\right]$$
$$- \frac{t_f + 2t_s - 2(t - t_1)}{2t_f}\left[1 + erf\left(-\frac{\sqrt{2}}{2}\delta\right)\right]$$

(34)

• • • • • •

n-th mining unit:

$$F\left(t - \sum_{n=1}^{n-1} t_n\right) = \frac{1}{2}\left[erf\left(\frac{\sqrt{2}\delta}{t_f}\left(t - \sum_{n=1}^{n-1} t_n - t_s - \frac{t_f}{2}\right)\right) + 1\right]$$
$$- \frac{t_f + 2t_s - 2\left(t - \sum_{n=1}^{n-1} t_n\right)}{2t_f}\left[1 + erf\left(-\frac{\sqrt{2}}{2}\delta\right)\right]$$

(35)

According to the dynamic prediction principle, the settlement prediction model at any point on the surface at any time can be calculated by Eq. (32), that is,

$$W(x, y, t) = W_1(x, y)F(t_1) + W_2(x, y)F(t - t_1) + \cdots$$
$$+ W_n(x, y)F\left(t - \sum_{n=1}^{n-1} t_n\right)$$

(36)

In the formula, $W_1(x, y)$ is the formula for calculating the maximum subsidence contributed to the ground surface by the first dynamic unit after mining, and $F_1(t)$ is the time function value corresponding to the first dynamic unit. The meanings of other formulas can be known by analogy. $W_1(x, y)$, $W_2(x, y)$, $\cdots$, and $W_n(x, y)$ can be calculated according to Eq. (19). Similarly, the dynamic prediction formulas of surface tilt, curvature, horizontal displacement, and horizontal deformation can

be obtained by analogy with the corresponding formulas of the Boltzmann function prediction model.

Predicted parameter inversion

Both the Boltzmann function prediction model and the transformed normal distribution time function are highly nonlinear and contain many related parameters. Considering that it is relatively difficult to use conventional methods to solve these parameters, we implemented that an intelligent optimization algorithm will be used in the research. Particle swarm optimization (PSO) (Zhang et al. 2019b; Li et al. 2019b) algorithm has a strong local search ability and fast convergence speed, but it easily generates a local extremum, and its global optimization ability is relatively poor. However, the shuffled frog leaping algorithm (SFLA) (Cui et al. 2012; Luo et al. 2010) is an intelligent optimization algorithm with internal and external double iterations that has a strong global search ability, but its disadvantages include an overly complex calculation and slow convergence speed. Therefore, PSO and SFLA can be combined (PSO-SFLA) to achieve global optimization and fast convergence. PSO-SFLA is used to solve the relevant parameters in the dynamic prediction model. The main steps were as follows:

PSO-SFLA parameter setting. Given the number of frogs N, the number of sub-populations m, the number of frogs contained in a single sub-population n, the learning factors c_1 and c_2, and the total number of iterations of the SFLA algorithm G_{max}

PSO algorithm initialization. Assign the number of sub-population and the number of particles in the sub-population, establish an eight-dimensional solution space $P = [q, b, \theta_0, \tan\beta, S_1, S_2, S_3, S_4]$, and randomly generate k particles in each dimension after setting the value range of each parameter.

Build fitness function. Let W_l be the measured subsidence value and W_i be the predicted subsidence value. Based on the sum of the least square difference between the predicted value and the measured value, the fitness function is obtained as follows:

$$f = \sum (W_l - W_i)^2$$

(37)

Each sub-population is optimized according to the particle swarm iteration mode, and the fitness is calculated to obtain the optimal particle L_b.
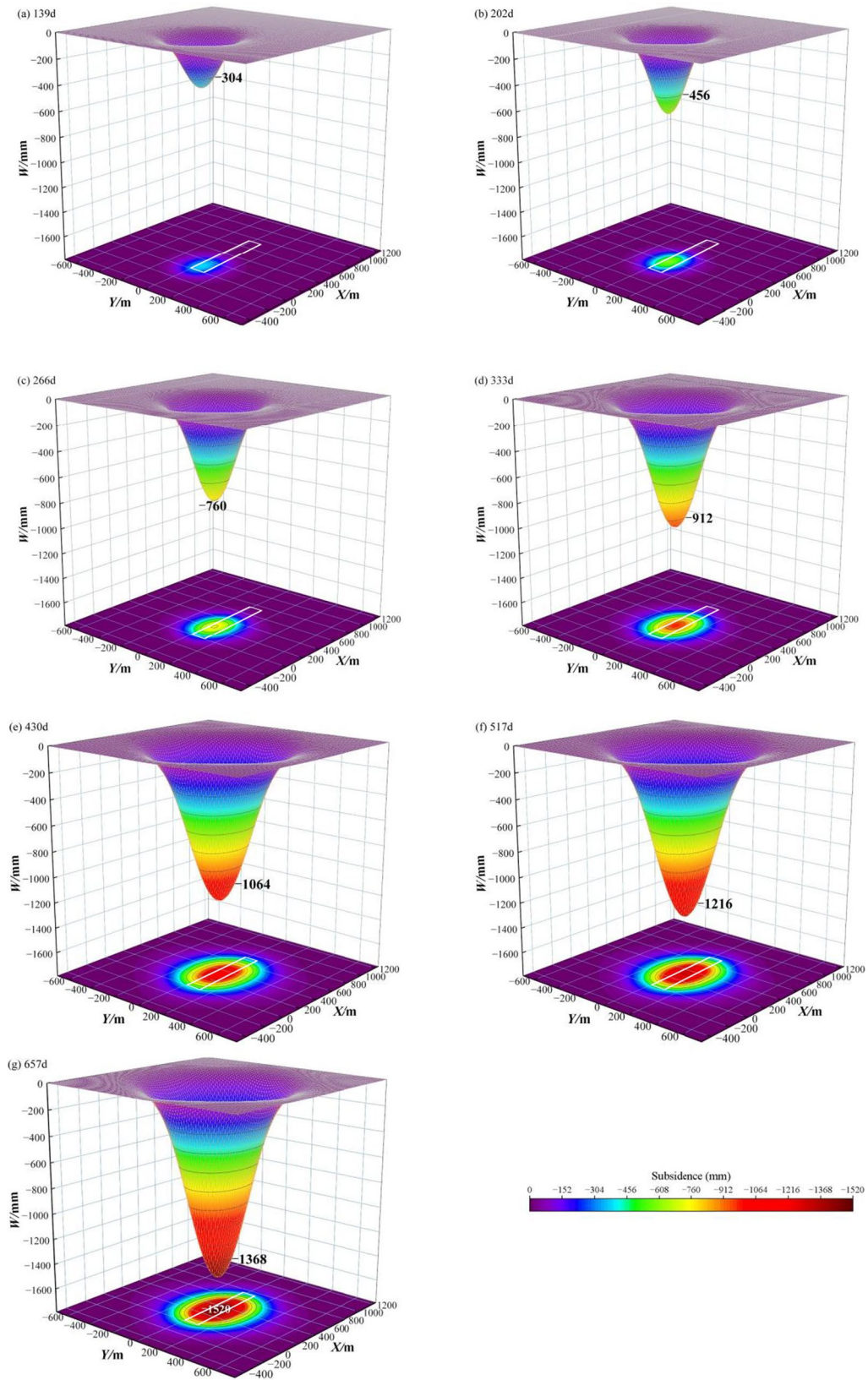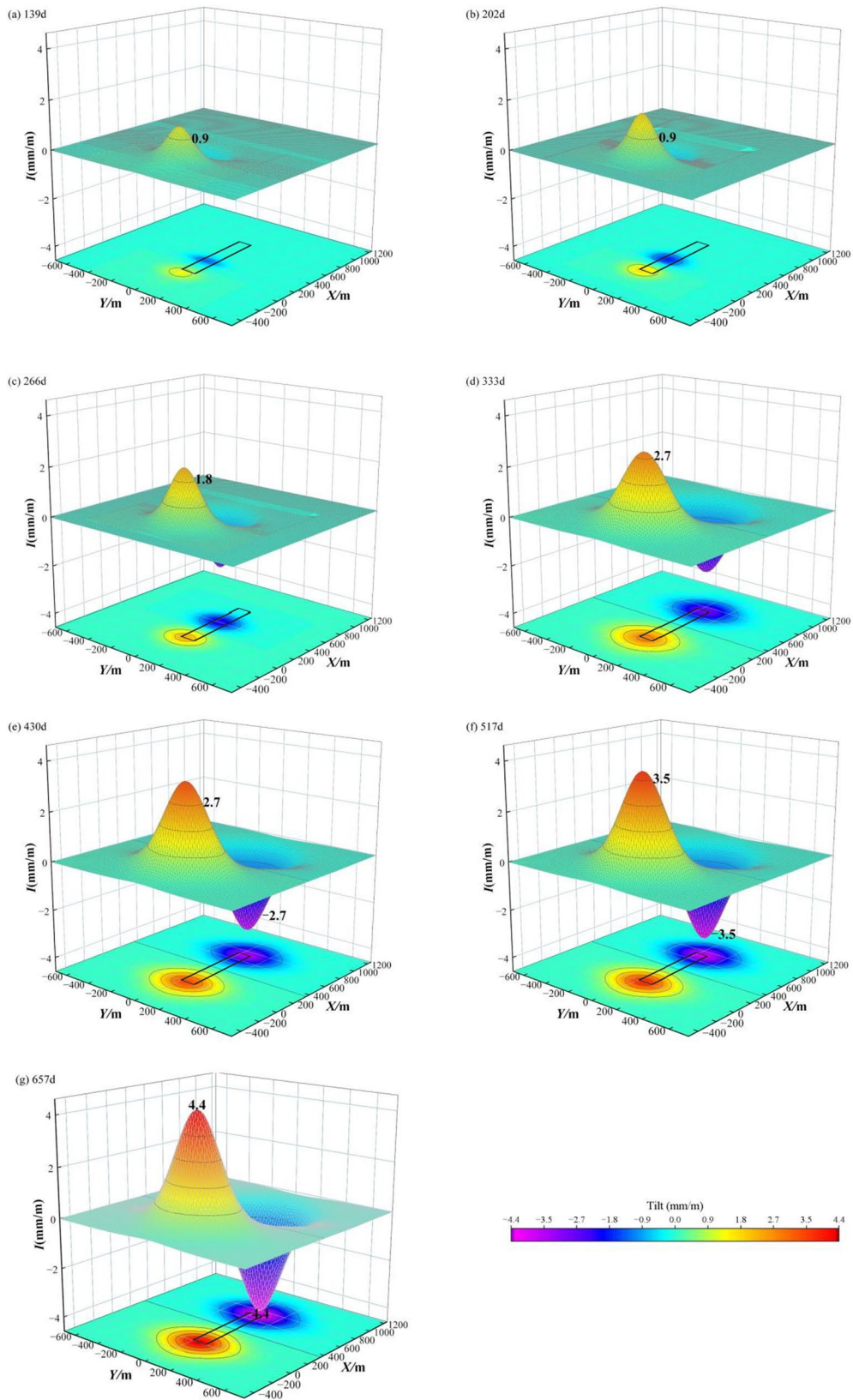
Fig. 10 3D dynamic subsidence and its projection map

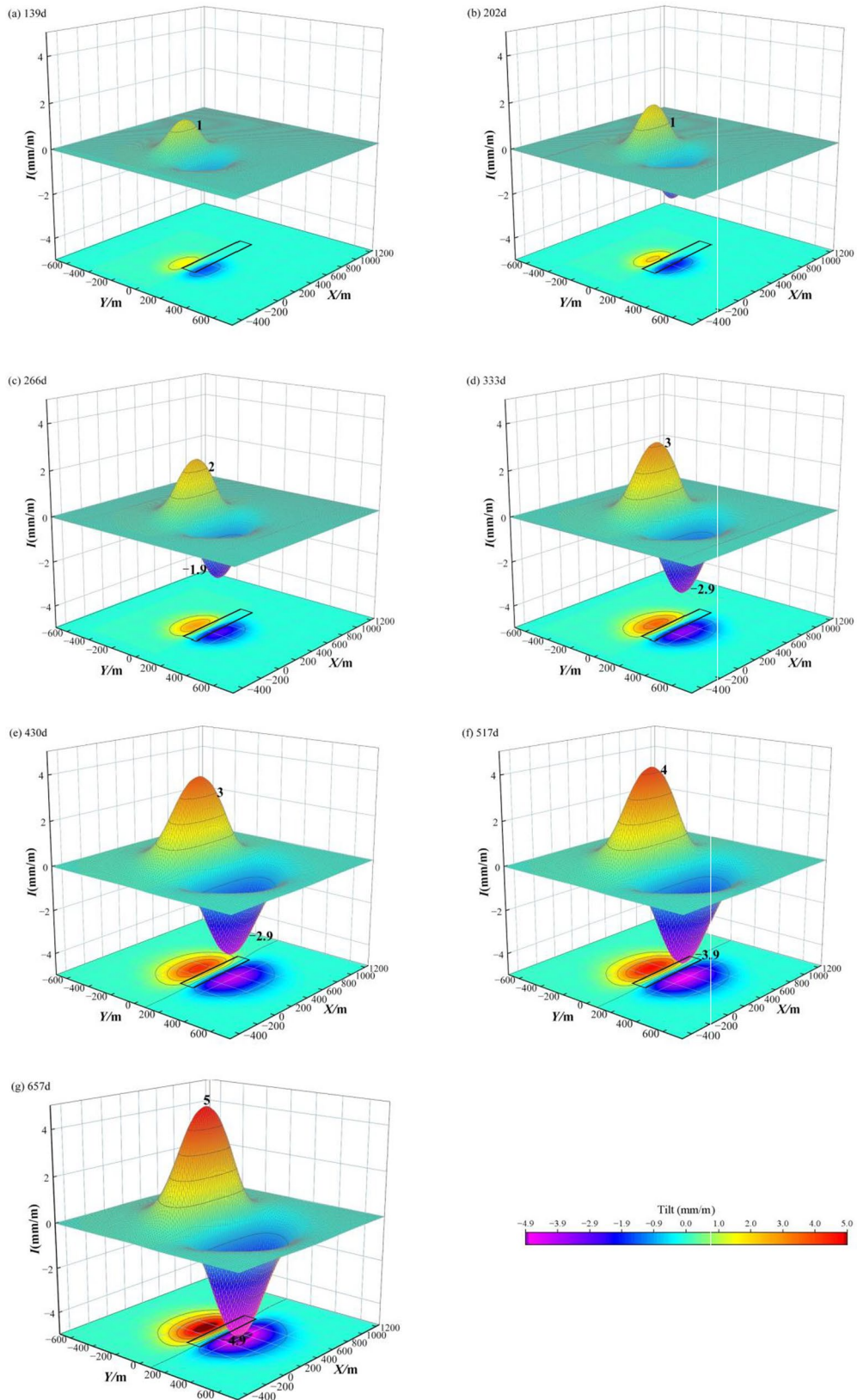**Fig. 11** Dynamic 3D tilt along strike and its projection map

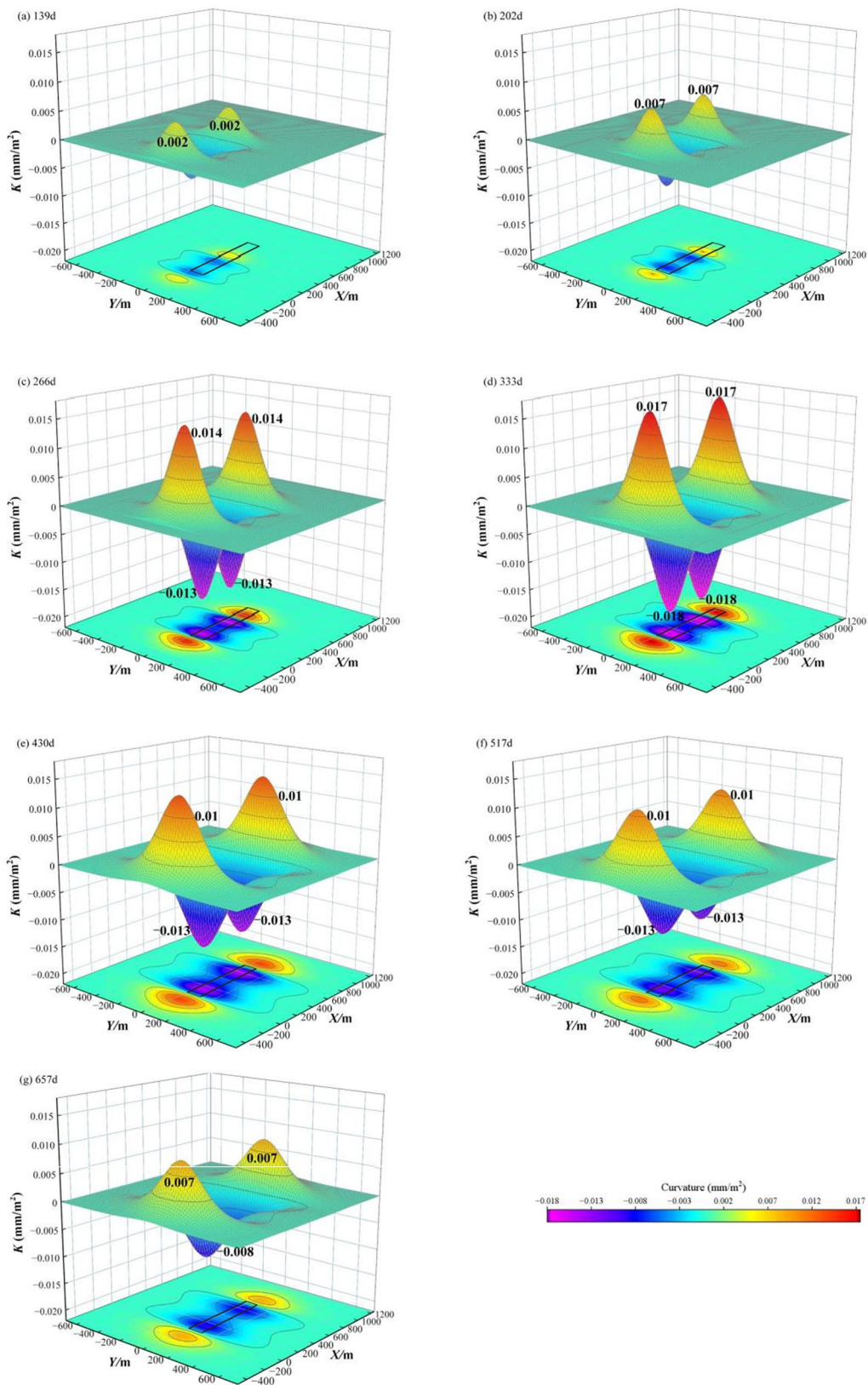**Fig. 12** Dynamic 3D tilt along the inclination and its projection map

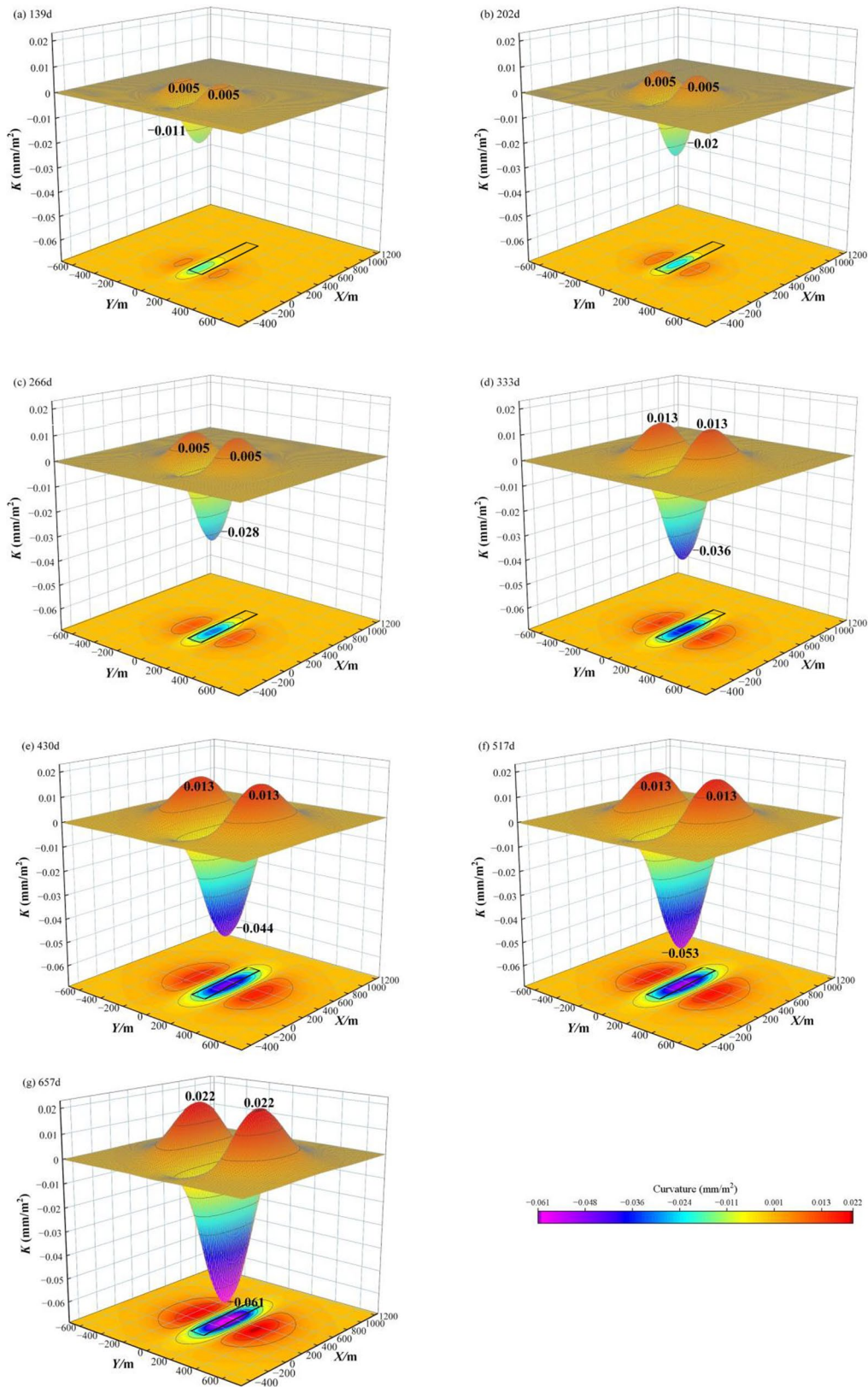**Fig. 13** Dynamic 3D curvature along strike and its projection map

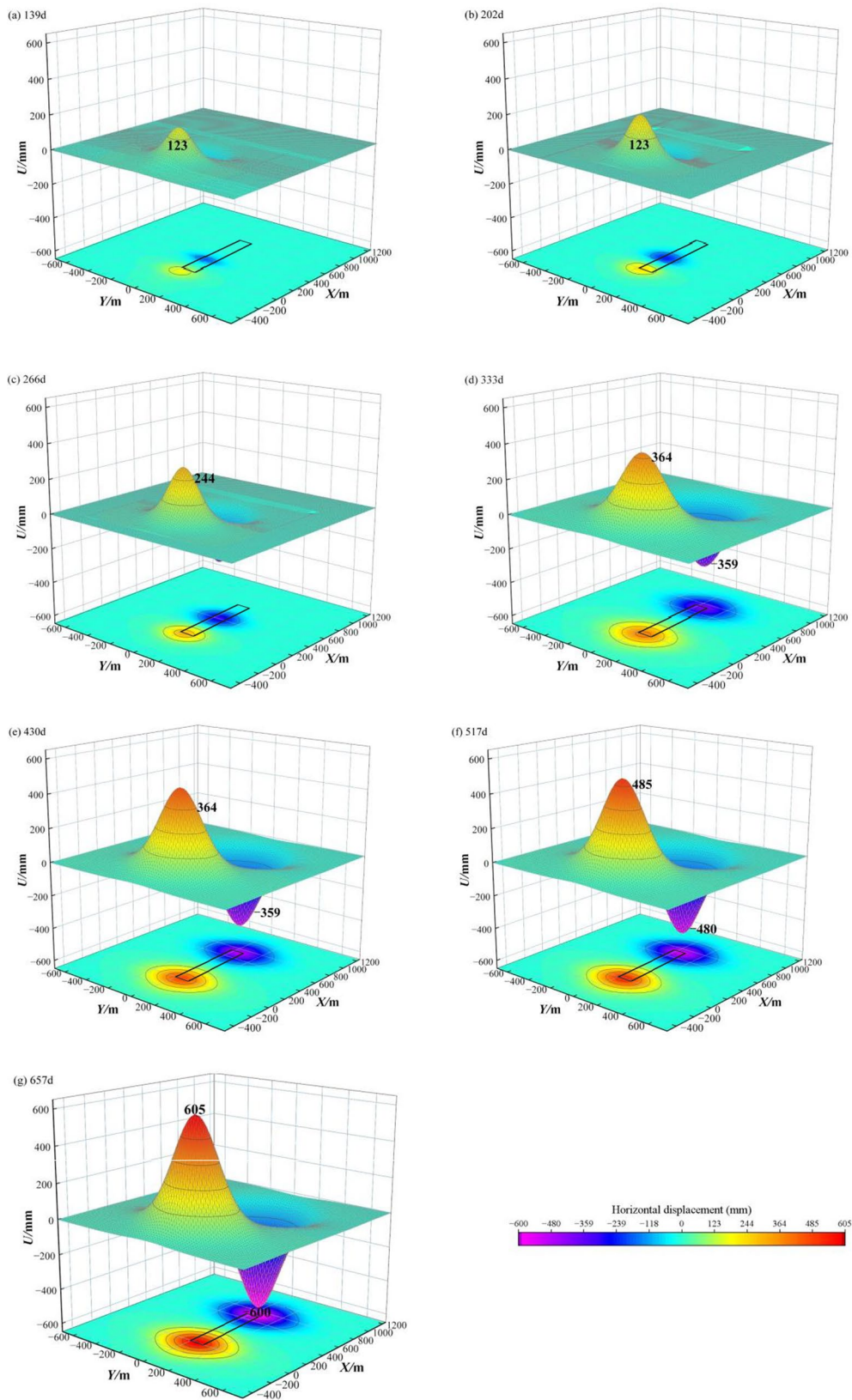**Fig. 14** Dynamic 3D curvature along the inclination and its projection map

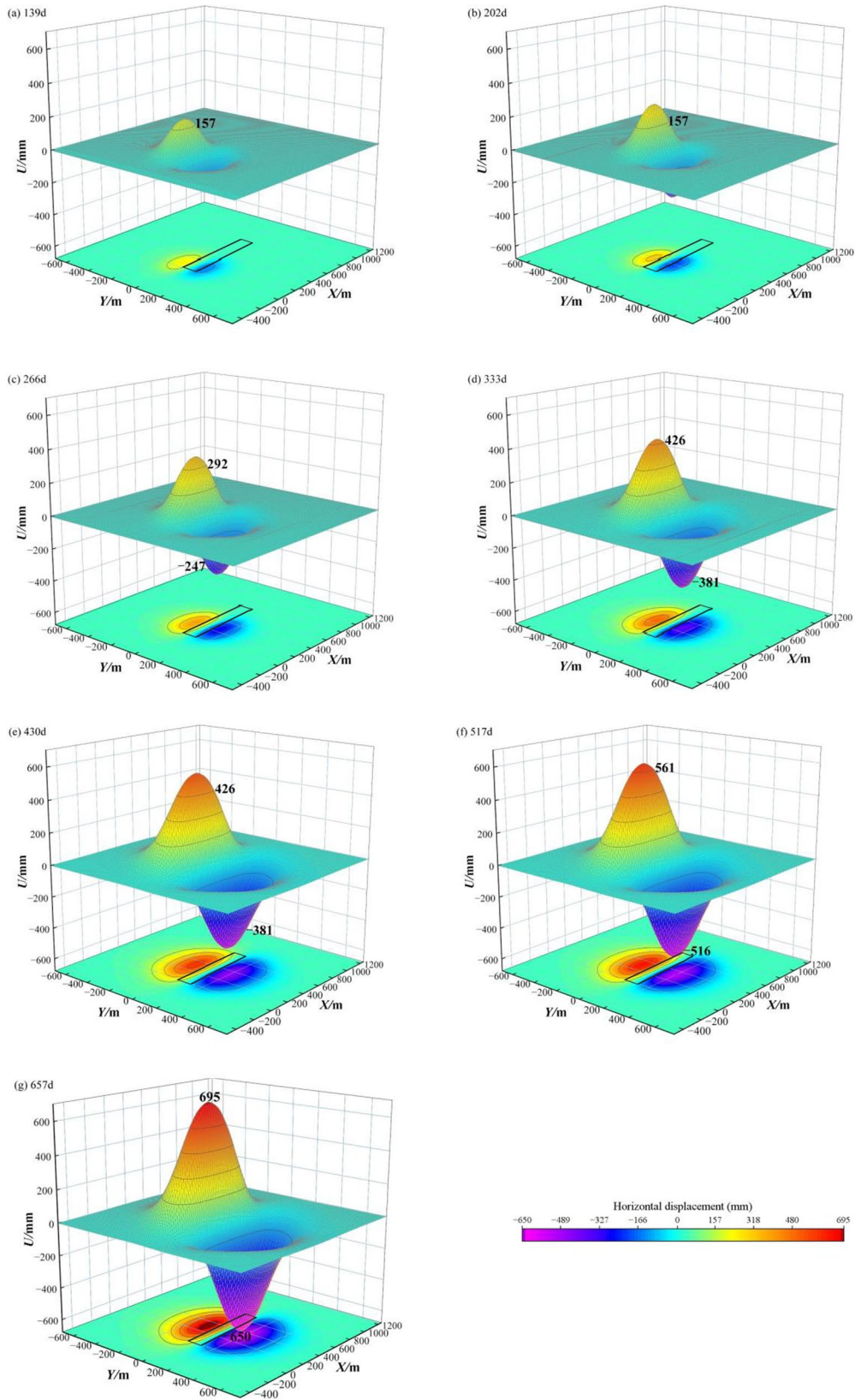**Fig. 15** Dynamic 3D horizontal displacement along strike and its projection map

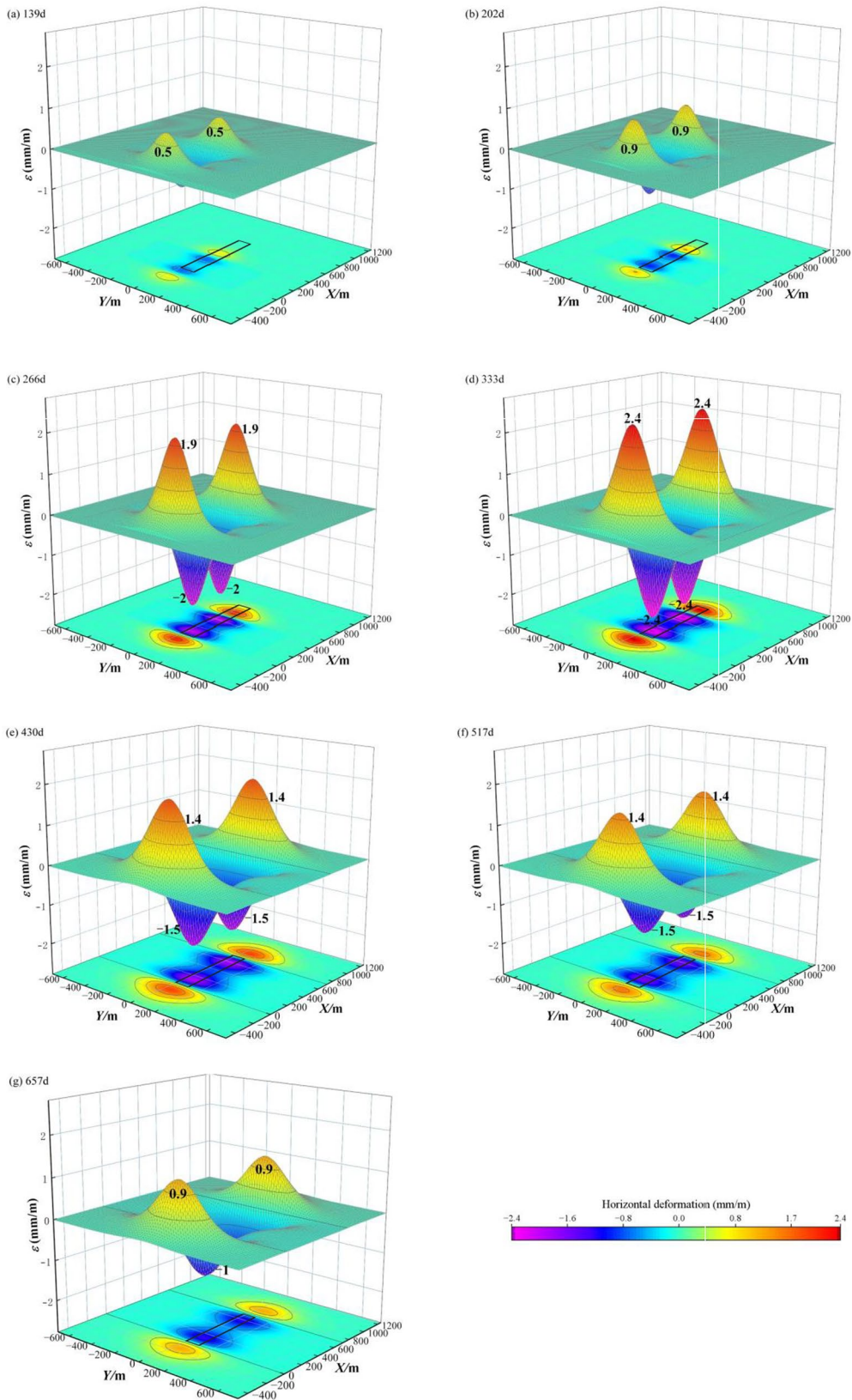**Fig. 16** Dynamic 3D horizontal displacement along the inclination and its projection map

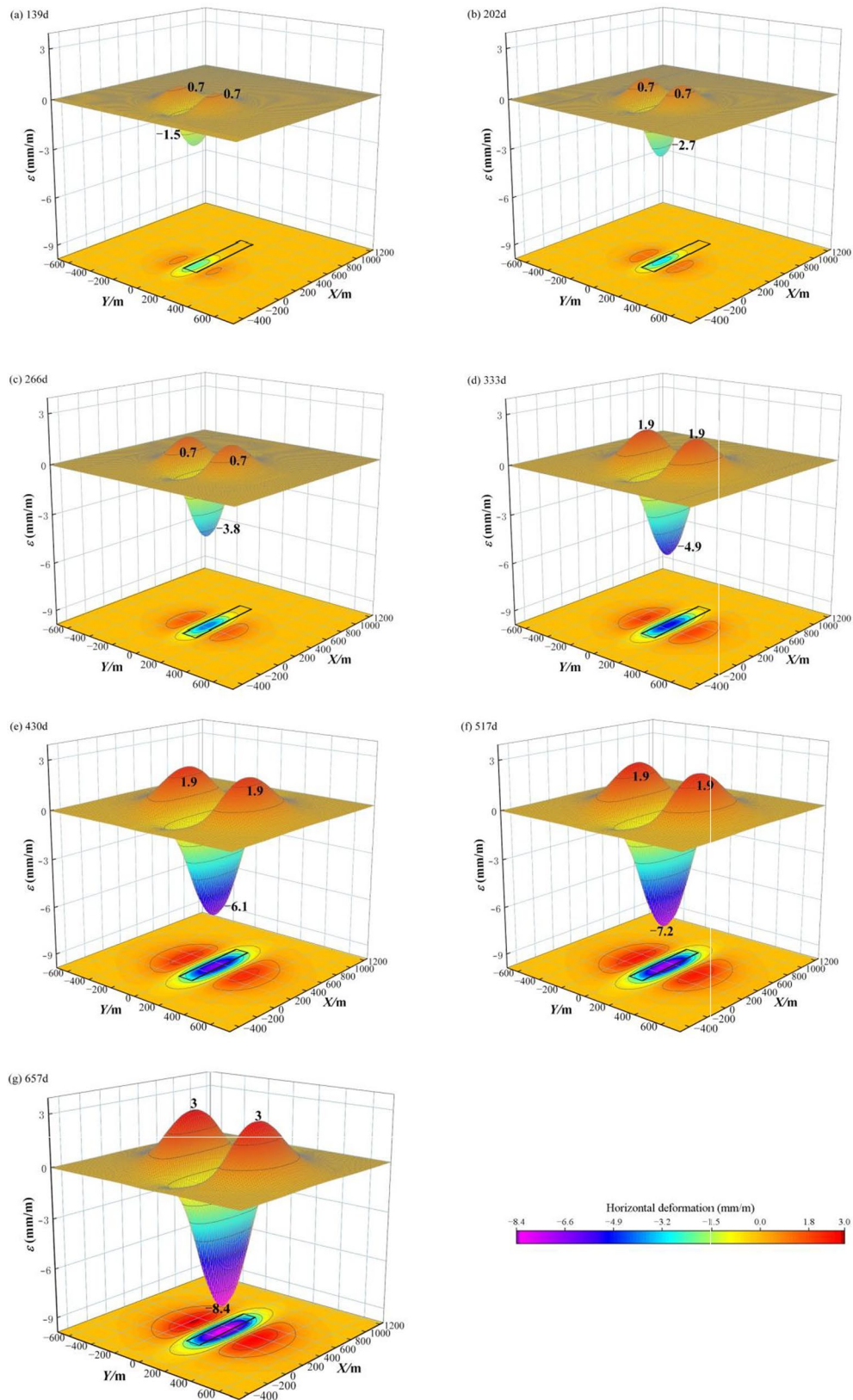**Fig. 17** Dynamic 3D horizontal deformation along strike and its projection map

Fig. 18 Dynamic 3D horizontal deformation along the inclination and its projection map

Fig. 19 Comparison of predicted subsidence and measured subsidence of strike and dip observation lines
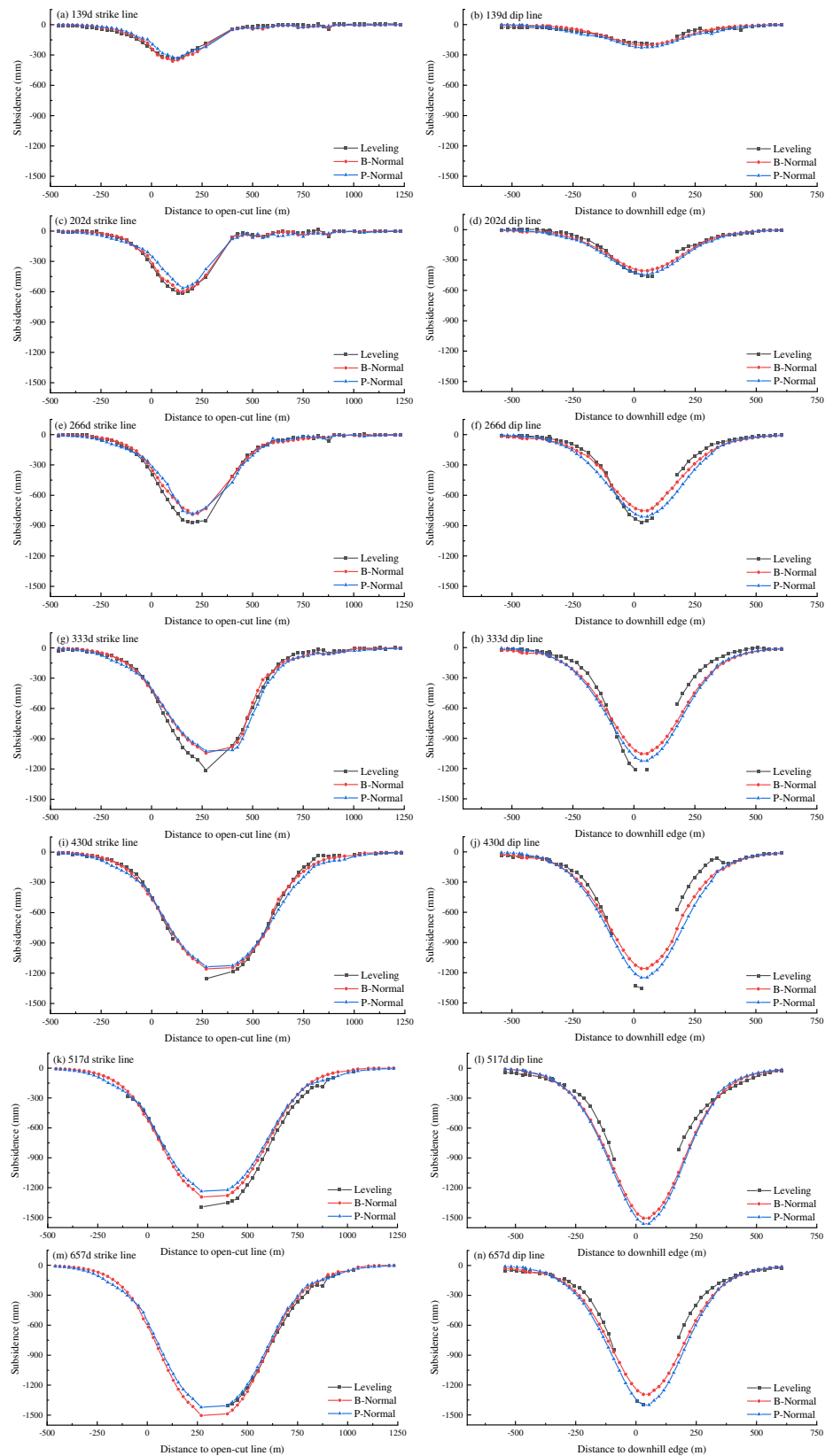
Table 2 Comparison of dynamic subsidence prediction accuracy between B-normal model and P-normal model

Predicted time (day)	B-normal				P-normal			
	Strike *W*		Dip *W*		Strike *W*		Dip *W*	
	RMSE (mm)	RRMSE	RMSE (mm)	RRMSE	RMSE (mm)	RRMSE	RMSE (mm)	RRMSE
139	16.2	4.8%	18.5	9.4%	22.4	6.7%	24.3	12.4%
202	15.7	2.5%	27.7	6.0%	42.1	6.8%	31.7	6.8%
266	41.1	4.7%	48.8	5.6%	51.6	5.9%	64.4	7.4%
333	52.8	4.4%	88.7	7.3%	61.5	5.1%	91.3	7.5%
430	28.7	2.3%	89.4	6.6%	49.1	3.9%	117.0	8.6%
517	66.1	4.7%	73.1	5.2%	85.1	6.1%	96.8	6.9%
657	38.9	2.8%	83.9	5.9%	42.3	3.0%	99.4	7.0%
Mean	37.1	3.8%	61.4	6.6%	50.6	5.4%	75.0	8.1%
Improved accuracy	26.7%	30.0%	18.1%	18.8%				

The position and velocity of each particle are updated according to the step size updating method of the particle swarm optimization algorithm.

The optimal particle L_b obtained in (3) is transformed into an individual frog of SFLA, and the fitness is calculated according to the fitness function and arranged in descending order according to the fitness value of the frog, to record the global optimal solution in each sub-population.

Intragroup iterative evolution. Set the moving distance of frogs for grouping, and then perform iterative evolution within the group. If the new solution reduces the fitness function value, the original solution is replaced by the new solution. Otherwise, replace the optimal solution in the group with the global optimal solution, and repeat the above steps. If the above steps fail to minimize the fitness function, a group of new solutions will be randomly generated to replace the worst solution in the group, and then, a local depth search will be performed.

Global hybrid search. After the number of iterative evolution reached the peak, the frogs in each group were remixed and sorted according to the fitness function value. If the set maximum number of iterations or accuracy requirements are reached, stop searching and output a group of optimal solutions; otherwise, return to step (4) to continue the cycle.

The technical route of model parameter inversion is shown in Fig. 8.

Application example of dynamic prediction of arbitrary point displacement deformation

Overview of the study area

The 8102 working face in 81 mining areas of the Guobei coal mine is selected as the research object in the test. It is located in Guoyang County, Bozhou City, Anhui Province, China. The terrain of the mining area is relatively flat. There are many roads, villages, and other buildings on the surface, which is also traversed by rivers. The positions of the working face and the surface observation line are shown in Fig. 9, and the relevant parameters are shown in Table 1. 8101, the successor of the 8102 working face, began mining in February 23, 2008, which had a certain impact on the later displacement and deformation of 8102 working face.

The dynamic prediction parameters of working face 8102 are as follows: subsidence coefficient $q = 0.7$, horizontal displacement coefficient $b = 0.34$, mining influence propagation angle $\theta_0 = 89.5°$, main influence angle tangent $\tan\beta = 1.5$, strike left and right turning point offset $S_3 = S_4 = 60$ m, downhill turning point offset $S_1 = -20$ m, and uphill turning point offset $S_2 = 20$ m.

Subsidence dynamic prediction

Before dynamic prediction, we took the lower left corner of the 8102 working face as the coordinate origin; took the advancing direction and inclined uphill direction of the working face as the positive direction of the *x*-axis and the *y*-axis, respectively, to establish the working face coordinate system; and converted the coordinates of the working face and feature points to the working face coordinate system according to Eq. (38).

$$\begin{bmatrix} x' \\ y' \end{bmatrix} = \begin{bmatrix} x - x_0 \\ y - y_0 \end{bmatrix} \begin{bmatrix} \cos\varphi & \sin\varphi \\ -\sin\varphi & \cos\varphi \end{bmatrix} \tag{38}$$

where (x', y') is the coordinate under the working face coordinate system, (x, y) is the coordinate under the actual

Fig. 20 Comparison of predicted tilt and measured inclination of strike and inclination observation lines
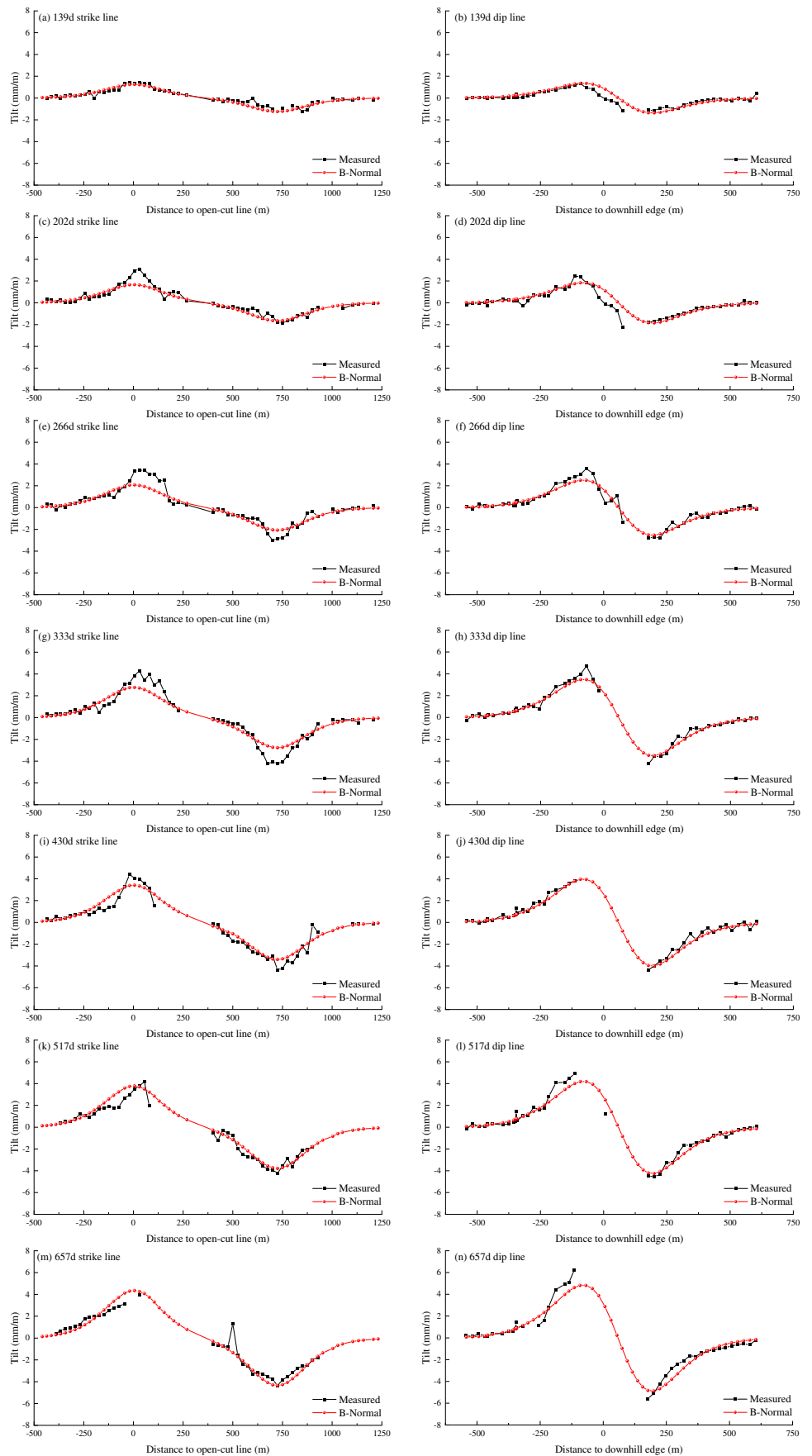
Table 3 Dynamic tilt prediction accuracy

Predicted time (day)	Strike I		Dip I	
	RMSE (mm/m)	RRMSE	RMSE (mm/m)	RRMSE
139	0.23	16.2%	0.30	25.1%
202	0.40	13.1%	0.45	12.5%
266	0.57	16.7%	0.40	14.3%
333	0.68	15.9%	0.34	7.1%
430	0.55	12.4%	0.30	6.8%
517	0.53	12.5%	0.44	8.9%
657	0.58	13.4%	0.55	8.8%
Mean	0.51	14.3%	0.39	11.9%

coordinate system, (x_0, y_0) is the coordinate of the origin of the working face coordinate system under the actual coordinate system, and φ is the angle from the actual coordinate system to the working face coordinate system counterclockwise.

After the coordinate conversion was completed, the time parameters δ, t_s, and t_f of the transformed normal distribution time function and the corresponding predicted parameters of the Boltzmann function prediction model were inverted by using the measured leveling data on the 657th day after the cutting of the working face and in combination with the parameter inversion method described in the "Predicted parameter inversion" section.

The inversion model parameters were used to predict the forward dynamics of surface displacement and deformation, and the corresponding predicted times were 139, 202, 266, 333, 430, 517, and 657 days after the cutting of the working face. The predicted dynamic 3D subsidence of the ground surface at each time and the corresponding 2D projection results are shown in Fig. 10. It can be seen from the figure that with the advance in the working face, the scope of the surface movement basin gradually expanded towards the mining direction, and the settlement value also gradually increased. After stopping mining in the working face, the surface continued to sink, because it was still in the active subsidence period. As of the 657th day after cutting, the maximum subsidence value in the center of the basin reached −1520 mm.

Tilt dynamic prediction

The 2D and 3D dynamic tilt prediction results along the strike direction of working face 8102 are shown in Fig. 11, and the 2D and 3D dynamic tilt prediction results along the dip direction are shown in Fig. 12. It can also be seen that the surface tilt also developed towards the mining direction. The tilt range and tilt value along the strike and dip

direction are gradually increased, showing the symmetrical distribution characteristics of equal size and opposite symbols. The difference was that the dip along the strike was −4.4~4.4 mm/m, and the range was mainly concentrated at the north and south ends of the goaf. The inclination along the dip direction was −4.9~5.0 mm/m, and the range is mainly concentrated on the east and west sides of the goaf.

Curvature dynamic prediction

The predicted results for the 2D and 3D dynamic curvature along the strike direction of the 8102 working face are shown in Fig. 13, and the predicted results for the 2D and 3D dynamic curvature along the dip direction are shown in Fig. 14. It can be seen from the figure that with the advance in the working face, the influence range of the curvature along the strike and dip directions gradually expanded. The curvature characteristics along the strike direction were mainly as follows: the north and south ends of the goaf had a positive curvature, and the center of the mobile basin had a negative curvature, which was distributed symmetrically from north to south. The maximum value of the curvature first increased and then decreased, and the maximum value of −0.018 mm/m² appeared on the 333th day, ranging from −0.018 to 0.017 mm/m². The curvature characteristics along the dip direction were mainly as follows: the curvature value gradually increased, with a positive curvature exists on the east and west sides of the goaf and a negative curvature exists in the center of the mobile basin, and the curvature value of the center of the mobile basin was significantly greater than that on both sides, ranging from −0.061 to 0.022 mm/m².

Horizontal displacement dynamic prediction

The predicted results for the 2D and 3D dynamic horizontal displacement of the 8102 working face along the strike direction are shown in Fig. 15, and the predicted results for the 2D and 3D dynamic horizontal displacement along the dip direction are shown in Fig. 16. It can be seen from the figures that the horizontal displacement deformation characteristics of the ground surface were similar to the tilt, and they are also developed in the mining direction. The horizontal displacement range and horizontal displacement value along the strike and dip directions are gradually increased, showing an approximate symmetrical distribution with similar size and opposite symbols. The difference was that the horizontal displacement along the strike direction was between −600 and 605 mm, and the range was mainly concentrated at the north and south ends of the goaf. The horizontal displacement along the dip

Fig. 21 Comparison of the predicted and measured curvatures of the strike and inclination observation lines
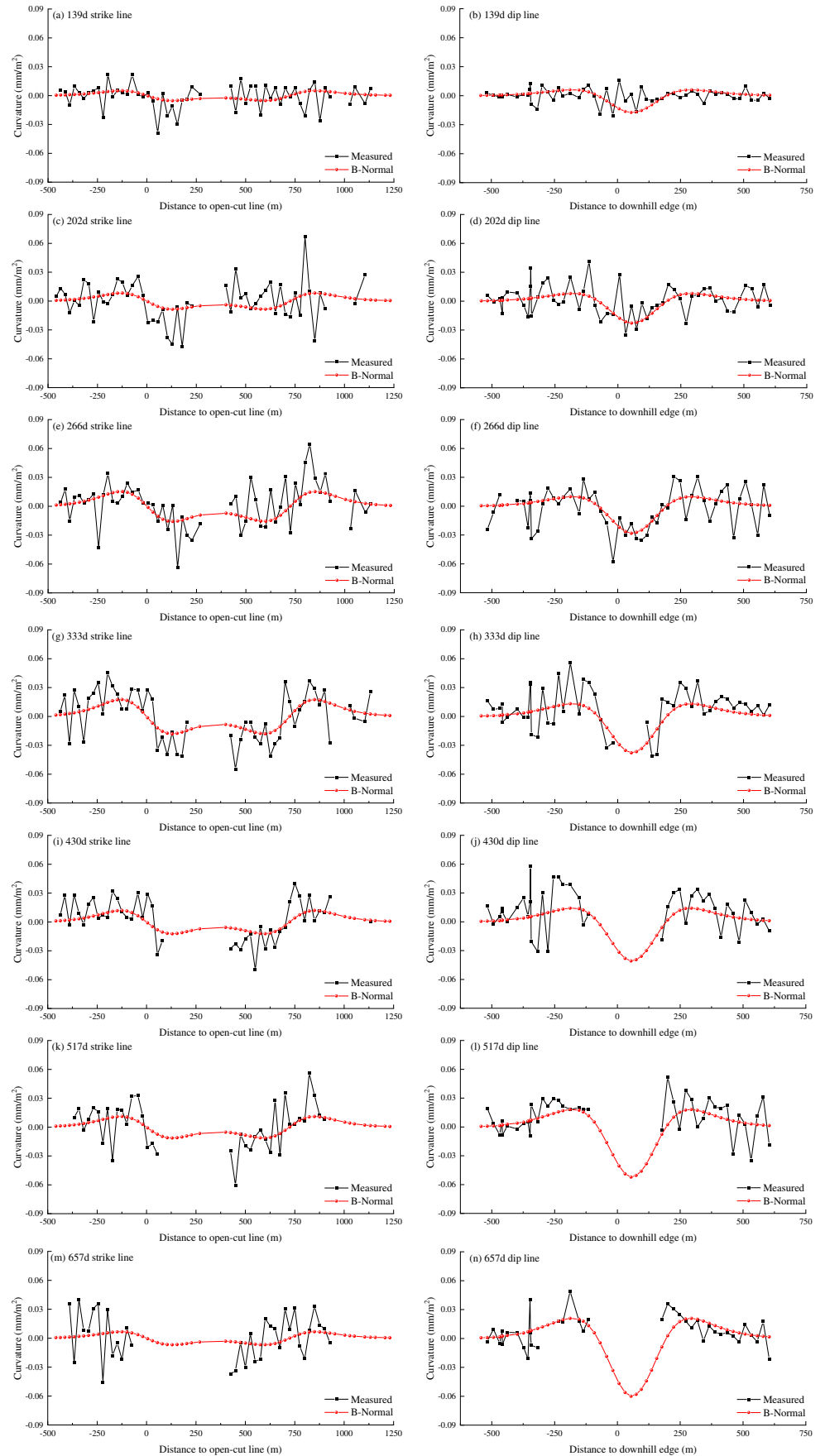
Table 4 Dynamic curvature prediction accuracy

Predicted time (day)	Strike K		Dip K	
	RMSE (mm/m^2)	RRMSE	RMSE (mm/m^2)	RRMSE
139	0.016	19.8%	0.009	31.4%
202	0.019	28.5%	0.014	24.6%
266	0.019	30.3%	0.017	28.8%
333	0.019	34.6%	0.018	31.6%
430	0.016	32.7%	0.020	35.5%
517	0.020	33.7%	0.016	31.0%
657	0.027	31.8%	0.014	29.4%
Mean	0.020	30.2%	0.016	30.3%

direction was between −650 and 695 mm, and the range was mainly concentrated on the east and west sides of the goaf.

Horizontal deformation dynamic prediction

The predicted results for the 2D and 3D dynamic horizontal deformation along the strike direction of the 8102 working face are shown in Fig. 17, and the predicted results for the 2D and 3D dynamic horizontal deformation along the dip direction are shown in Fig. 18.

It can be seen from the figures that the horizontal deformation characteristics of the surface were similar to the curvature. With the advance in the working face, the horizontal deformation range along the strike and dip direction gradually expanded. The horizontal deformation along the strike direction was mainly characterized by positive horizontal deformation at the north and south ends of the goaf and negative horizontal deformation at the center of the mobile basin, which was symmetrically distributed from north to south. The maximum value of horizontal deformation first increased and then decreased, and the maximum value of −2.4 mm/m appeared on the 333rd day, with a range of −2.4~2.4 mm/m. The horizontal deformation along the dip direction was characterized by a gradual increase in the horizontal deformation value, positive horizontal deformation at the east and west sides of the goaf, negative horizontal deformation at the center of the mobile basin, and a horizontal deformation value at the center of the mobile basin that was significantly greater than that at both sides, ranging from −8.4 to 3.0 mm/m.

Accuracy verification

Since the shape of the main section of the strike and dip of the working face can basically determine the shape of the mobile basin, the accuracy of the prediction results based on the mobile deformation in the main section is sufficient to represent the prediction accuracy of the whole basin. Therefore, the measured subsidence, tilt, curvature, horizontal displacement, and horizontal deformation values of the strike and inclination observation line of the 8102 working face at each predicted time could be compared with the dynamic predicted values to verify the accuracy of the B-normal dynamic prediction model. The accuracy was investigated by root mean square error (RMSE) and relative root mean square error (RRMSE). The calculation formulas are shown in formula (39) and formula (40), respectively.

$$\text{RMSE} = \sqrt{\frac{\sum_{m=1}^{n} \Delta_m^2}{n}} = \sqrt{\frac{\sum_{m=1}^{n} \left(W_{P_m} - W_{L_m}\right)^2}{n}} \tag{39}$$

$$\text{RRMSE} = \frac{\text{RMSE}}{W_{\max}} \tag{40}$$

where W_{P_m} is the predicted deformation value of benchmark m, W_{L_m} is the measured deformation value of benchmark m, and $W_{\max}$ is the measured maximum deformation value.

Accuracy analysis of dynamic subsidence prediction

To more intuitively reflect the prediction accuracy of the B-normal model and highlight its advantages over the existing models, the dynamic prediction model based on PIM and normal distribution time function (P-normal) has also been used to dynamically predict the subsidence of the strike and dip observation line of 8102 working face at the same prediction time. The comparison curve of the prediction results is shown in Fig. 19, and the precision of its statistics is shown in Table 2. It should be noted that some observation points on the south bank of the river cannot be accurately observed due to ponding in the surface subsidence basin after the mining of the working face was completed, and working face 8102, the successor to working face 8101, had been mined for 513 m on the 657th day after the cutting of working face 8102, which caused the observation points close to the working face 8101 to continue to subsidence. Therefore, these observation points were excluded from Fig. 19m and Fig. 19n corresponding to 657 days.

It can be seen from Table 2 that the prediction accuracy of the B-normal model was better than that of the P-normal model at each prediction time. On the strike observation line, the average RMSE and RRMSE of the predicted results of each phase of the B-normal model were 37.1 mm and 3.8%, respectively, which were 26.7% and 30.0% higher than those of the P-normal model. On the trend observation line, the average RMSE and RRMSE of the predicted results of the B-normal model

Fig. 22 Comparison of the predicted horizontal displacement and the measured horizontal displacement of the trend and inclination observation lines
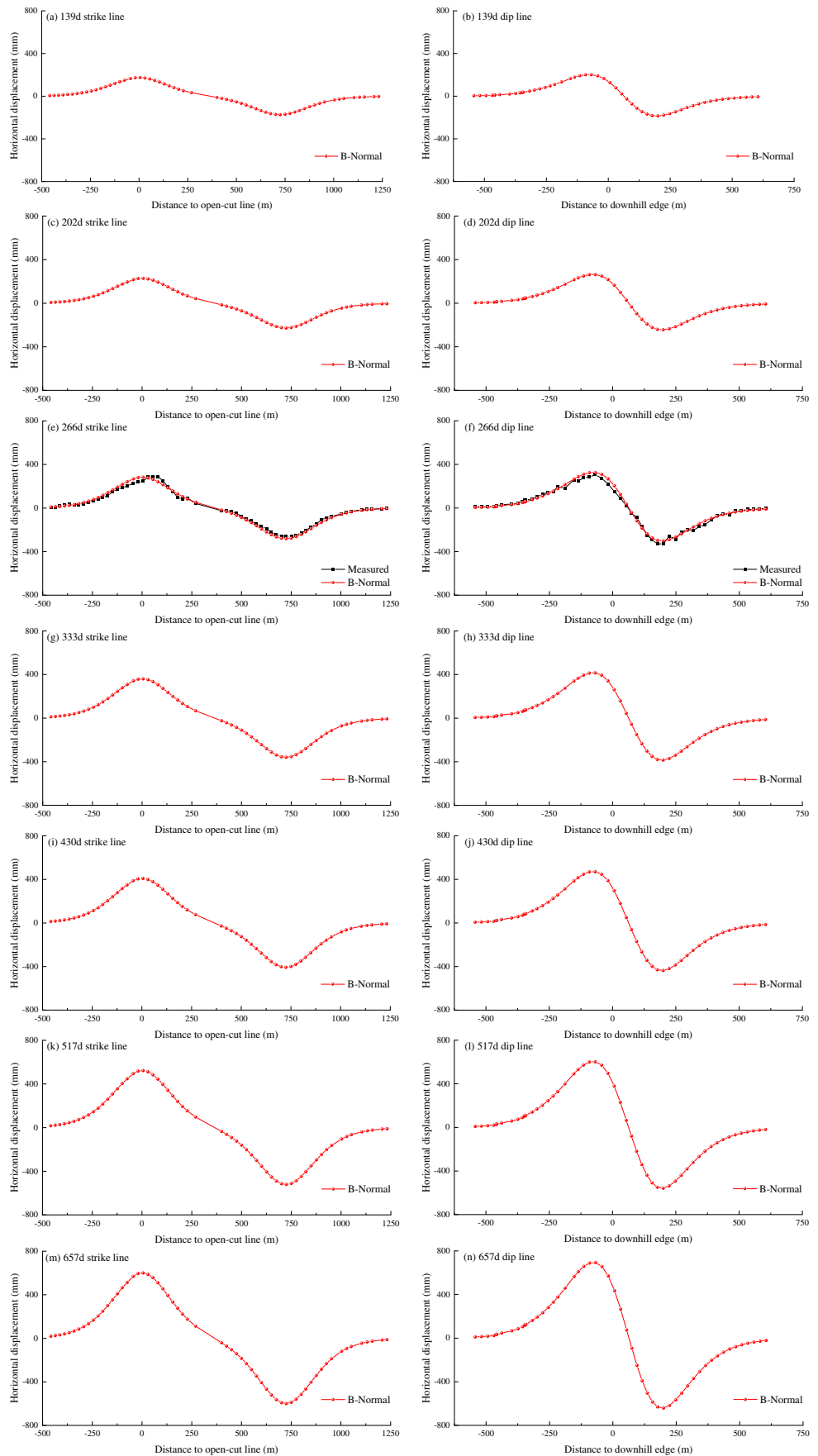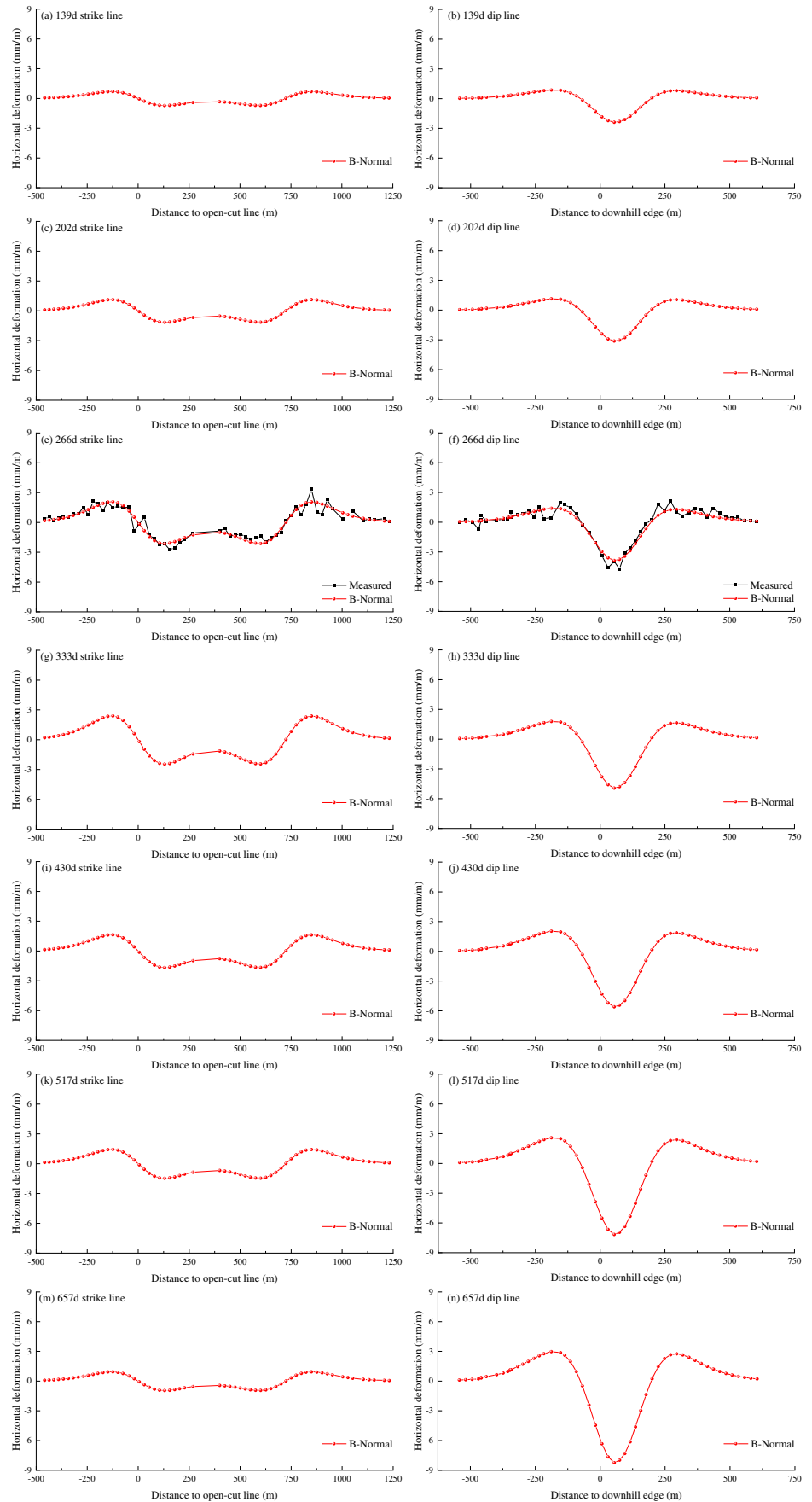
Fig. 23 Comparison of predicted horizontal deformation and measured horizontal deformation of strike and dip observation lines

in each period were 61.4 mm and 6.6%, respectively, which were 18.1% and 18.8% higher than those of the P-normal model, further verifying the reliability of the B-normal model.

Accuracy analysis of dynamic tilt prediction

We compared the predicted tilt of the strike observation line along the strike and dip observation line along and the dip of working face 8102 with the measured tilt. The comparison curve is shown in Fig. 20, and the statistical accuracy is shown in Table 3.

It can be seen from Table 3 that the average RMSE of the tilt on the strike and inclination observation lines at each predicted time was 0.51 mm/m and 0.39 mm/m, respectively, which was about 1/7~1/6 of the critical value of the grade I damage level (3 mm/m) of inclination. The average RRMSE of the inclination was 14.3% and 11.9%, respectively, both less than 15%, which meets the requirements of engineering application.

Accuracy analysis of dynamic curvature prediction

We compared the predicted curvature of the strike observation line along the strike and dip observation line along with the dip of working face 8102 with the measured curvature. The comparison curve is shown in Fig. 21, and the statistical accuracy is shown in Table 4.

It can be seen from Table 4 that the average RMSE of the curvature on the strike and dip observation lines at each predicted time was 0.020 mm/m^2 and 0.016 mm/m^2, respectively, and the average RRMSE was 30.2% and 30.3%, respectively. Although the RRMSE of the curvature was relatively large, the RMSE was relatively small, with an average value of 0.018 mm/m^2, which was only 1/11 of the critical value of the curvature I damage level (0.2 mm/m^2). It can be seen that the dynamic prediction accuracy of the B-normal model for curvature also fully meets the engineering application requirements.

Accuracy analysis of dynamic horizontal displacement prediction

The dynamic prediction results of the horizontal displacement of the strike observation line along the strike and the dip observation line along the dip of the 8102 working face are shown in Fig. 22. Since the measured coordinate data only existed on the 266th day after the cutting of the working face, we only produced a comparison curve between the predicted horizontal displacement and the measured horizontal displacement at this predicted time. The statistical accuracy is shown in Table 5.

Table 5 Predicted accuracy of dynamic horizontal displacement

Predicted time (day)	Strike U		Dip U	
	RMSE (mm)	RRMSE	RMSE (mm)	RRMSE
266	19.6	6.9%	21.5	6.5%

It can be seen from Table 5 that the average RMSE of the horizontal displacement on the strike and dip observation lines at 266 days at the predicted time was 19.6 mm and 21.5 mm, respectively, and the predicted accuracy reached the centimeter level. The average RRMSE was 6.9% and 6.5%, respectively, both less than 10%, which fully meets the engineering application needs.

Accuracy analysis of dynamic horizontal deformation prediction

The dynamic prediction results of the horizontal deformation along the strike observation line and the dip observation line of the 8102 working face are shown in Fig. 23. Similarly, since we measured coordinate data only on the 266th day after the cutting of the working face, we only produced a comparison curve between the predicted horizontal deformation and the measured horizontal deformation at this predicted time. The statistical accuracy is shown in Table 6. It can be seen from Table 6 that the average RMSE of the horizontal deformation on the strike and dip observation lines at the predicted time of 266 days was 0.49 mm/m and 0.46 mm/m, respectively. The average RRMSE was 14.7% and 9.7%, respectively, which meets the engineering application requirements.

Conclusions

To reveal the dynamic process of surface displacement and deformation caused by underground mining and predict the displacement and deformation values at any point and at any time in the mobile basin, a new dynamic prediction model for mining subsidence was proposed, and an intelligent optimization algorithm was introduced to solve the model parameters. The main conclusions of this study are as follows:

The convergence speed of the probability integral model is too fast at the edge. When using this model to predict the mining subsidence dynamics, the fitting effect

Table 6 Predicted accuracy of dynamic horizontal deformation

Predicted time (day)	Strike ε		Dip ε	
	RMSE (mm/m)	RRMSE	RMSE (mm/m)	RRMSE
266	0.49	14.7%	0.46	9.7%

with the subsidence basin boundary is often poor. The Boltzmann function model is similar to the probability integral model, and the convergence speed at the edge is relatively slow, which is more in line with the general law of mining subsidence.

Based on the Boltzmann function model and the transformed normal distribution time function, a prediction model for the dynamic displacement and deformation of any point on the surface during coal mining was constructed, and the calculation formulas for the displacement and deformation of the strike, dip, main section, and any point on the surface were provided.

The parameters of the dynamic prediction model were inversed by using the PSO-SFLA algorithm in combination with the measured surface data. The B-normal dynamic prediction model was applied to engineering practice to verify its reliability. The prediction results showed that the model can realize the high-precision dynamic prediction of the subsidence (W), tilt (I), curvature (K), horizontal displacement (U), and horizontal deformation (ε) of any point on the surface of the goaf and can better reflect the dynamic process of mining subsidence, thus fully meeting the practical application needs of engineering.

Declarations

Ethics approval Not applicable

Consent to participate Not applicable

Consent for publication Not applicable

Competing interests The authors declare no competing interests.

References

Adhelacahya K (2020) Ilma AZ (2021) Determination of neutron flux viewed from the Maxwell-Boltzmann's statistical distribution using numerical approach. Seminar Nasional Fisika (SNF) Unesa. https://doi.org/10.1088/1742-6596/1805/1/012046

Chang ZQ, Wang JZ, Chen M, A ZR, Yao Q (2015) A novel ground surface subsidence prediction model for sub-critical mining in the geological condition of a thick alluvium layer. Front Earth Sci 9(2): 330-341. https://doi.org/10.1007/s11707-014-0467-2

Chen YL, Zhou B, Li XB (2012) Mineral target prediction based on Boltzmann machines. Prog Geophy 27(01):179–185. https://doi.org/10.6038/j.issn.1004-2903.2012.01.020

Chi SS, Wang L, Yu XX, Fang XJ (2021a) Research on prediction model of mining subsidence in thick unconsolidated layer mining area. IEEE Access 9:23996–24010. https://doi.org/10.1109/ACCESS.2021.3056873

Chi SS, Wang L, Yu XX, Lv WC, Fang XJ (2021b) Research on dynamic prediction model of surface subsidence in mining areas with thick unconsolidated layers. Energ Explor Exploit 39:927–943. https://doi.org/10.1177/0144598720981645

Cui WH, Liu XB, Wang W, Wang JS (2012) Survey on shuffled frog leaping algorithm. Control Decision 27(4):481-486+93 https://doi.org/CNKI:SUN:KZYC.0.2012-04-002

Cui XM, Miu XX, Zhao YL, Jin RP (1999) Discussion on the time function of time dependent surface movement. J China Coal Soc 5:453–456 https://doi.org/CNKI:SUN:MTXB.0.1999-05-001

Gao C, Xu NZ, SunWM DWN, Han KM (2020) Dynamic surface subsidence prediction model based on Bertalanffy time function. J China Coal Soc 45(8):2740–2748. https://doi.org/10.13225/j.cnki.jccs.2019.0725

Gonzalez-nicieza C, Alvarez-fernandez MI, Menendez-diaz A (2007) The influence of time on subsidence in the Central Asturian Coalfield. Bull Eng Geol Environ 66(3):319–329. https://doi.org/10.1007/s10064-007-0085-2

Hu QF, Cui XM, Liu WK, Feng RM, Ma TJ, Li CY (2022a) Quantitative and dynamic predictive model for mining-induced movement and deformation of overlying strata. Eng Geol 311:106876. https://doi.org/10.1016/j.enggeo.2022.106876

Hu QF, Deng XB, Feng RM, Li CY, Wang XJ, Tong J (2015) Model for calculating the parameter of the Knothe time function based on angle of full subsidence. Int J Rock Mechan Mining Sci 78:19–26. https://doi.org/10.1016/j.ijrmms.2015.04.022

Hu QF, Cui XM, Liu WK, Feng RM, Ma TJ, Yuan DB (2022b) Knothe time function optimization model and its parameter calculation method and precision analysis. Minerals 12(6). https://doi.org/10.3390/min12060745

Huang SZ, Huang XX, Qin Q (2020) On the origin and derivation of normal distribution. Guide Sci Educ 13:41–43. https://doi.org/10.16400/j.cnki.kjdks.2020.05.021

Jiang C, Wang L, Yu XX (2021) Retrieving 3D large gradient deformation induced to mining subsidence based on fusion of Boltzmann prediction model and single-track InSAR earth observation technology. IEEE Access 9:87156–87172. https://doi.org/10.1109/ACCESS.2021.3089160

Li CY, Gao YG, Cui XM (2016) Progressive subsidence prediction of ground surface based on the normal distribution time function. Rock Soil Mech 37(S1):108–116. https://doi.org/10.16285/j.rsm.2016.S1.014

Li CY, Gao YG, Cui XM, Yuan DB, He R (2019a) Spatiotemporal evolution of surface subsidence induced by fully-mechanized thick coal underground mining in Yunjialing colliery. J Mining Safety Eng 36:37-43+50. https://doi.org/10.13545/j.cnki.jmse.2019.01.006

Li CY, Zhao L, Li M, Zhao YL, Cui XM, Cai HB (2020) Prediction of surface progressive subsidence and optimization of predicting model parameters based on logistic time function. J Safety Environ 20(06):2202–2210. https://doi.org/10.13637/j.issn.1009-6094.2019.1105

Li H, Zha J, Guo G (2019b) A new dynamic prediction method for surface subsidence based on numerical model parameter sensitivity. J Clean Prod 233:1418–1424. https://doi.org/10.1016/j.jclepro.2019.06.208

Li JY, Wang L (2021) Mining subsidence monitoring model based on BPM-EKTF and TLS and its application in building mining damage assessment. Environ Earth Sci 80:396–414. https://doi.org/10.1007/s12665-021-09704-5

Li SX (2019) Application of particle swarm optimization algorithm based on simulated annealing in function optimization. J Shenyang Univ Technol 41(6):664–668. https://doi.org/10.7688/j.issn.1000-1646.2019.06.13

Liu C, Li H, Mitri H (2019) Effect of strata conditions on shield pressure and surface subsidence at a longwall top coal caving working face. Rock Mech Rock Eng 52(5):1523–1537. https://doi.org/10.1007/s00603-018-1601-3

Liu F, Hu F (2003) A preliminary study on the construction of atmospheric dynamic models with lattice Boltzmann method. Acta Meteorol Sinica 3:267–274. https://doi.org/10.3321/j.issn:0577-6619.2003.03.002

Liu SL, Zhao WG, Qin SL, Chen LJ, Zhang Y (2011) Prediction on ultimate bearing capacity of pile based on Boltzmann function. J Civil Eng Manag 28(04):30-33+57. https://doi.org/10.3969/j.issn.2095-0985.2011.04.007

Luo JP, Li X, Chen MR (2010) The Markov model of shuffled frog leaping algorithm and its convergence analysis. Acta Electr Sinica 38(12):2875–2880 http://ir.calis.edu.cn/hdl/244041/2176

Nie L, Wang H, Xu Y, Li ZC (2014) A new prediction model for mining subsidence deformation: the arc tangent function model. Nat Hazards 75(3):2185–2198. https://doi.org/10.1007/s11069-014-1421-z

Shi J, Yang Z, Wu L, Qiao SY (2021) Improving the robustness of the MTI-estimated mining-induced 3D time-series displacements with a logistic model. Remote Sens 13(18). https://doi.org/10.3390/rs13183782

Unlu T, Akcin H, Yilmaz O (2013) An integrated approach for the prediction of subsidence for coal mining basins. Eng Geol 166:186–203. https://doi.org/10.1016/j.enggeo.2013.07.014

Wang J, Yang KM, Wei XP, Shi XY, Yao SY (2022) Prediction of longwall progressive subsidence basin using the Gompertz time function. Rock Mech Rock Eng 55(1):379–398. https://doi.org/10.1007/s00603-021-02664-z

Wang L, Teng CQ, Jiang KG, Jiang C, Zhu SJ (2021a) D-InSAR monitoring method of mining subsidence based on Boltzmann and its application in building mining damage assessment. KSCE J Civil Eng 26(1):353–370. https://doi.org/10.1007/s12205-021-1042-5

Wang N, Wu K, Liu J, An SK (2013) Model for mining subsidence prediction based on Boltzmann function. J China Coal Soc 38(8):1352–1356. https://doi.org/10.13225/j.cnki.jccs.2013.08.018

Wang XH (2016) Study on surface dynamic subsidence prediction method based on negative exponential method and Weibull time series function. Taiyuan Univ Technol. https://doi.org/10.7666/d.D01007797

Wang YT, Liu XP, Mao XG, Cao XY, Tian YZ (2021b) Research on prediction model of surface dynamic subsidence of mined-out region based on Usher time function. Coal Sci ogy 49(9):145–151. https://doi.org/10.13199/j.cnki.cst.2021.09.021

Zhang B, Cui XM, Hu QF (2016) Study on normal distributed time function model to dynamically predict mining subsidence. Coal Sci Technol 44(4):140-145+74. https://doi.org/10.13199/j.cnki.cst.2016.04.028

Zhang GJ, Yan W, Jiang KG (2021) Inversion method for the prediction parameters of mining subsidence based on the PB combination prediction model of variable weight. J Mining Strat Control Eng 3(1):87–95. https://doi.org/10.13532/j.jmsce.cn10-1638/td.20200714.001

Zhang K, Hu HF, Lian XG, Cai YF (2019a) Optimization of surface dynamic subsidence prediction normal time function model. Coal Sci Technol 47(09):235–240. https://doi.org/10.13199/j.cnki.cst.2019.09.030

Zhang XL, Wang QF, Ji WL (2019b) An improved particle swarm optimization algorithm for adaptive inertial weights. Microelectr Comp 36(03):66–70 https://doi.org/CNKI:SUN:WXYJ.0.2019-03-014

Zhang B, Zhao YL, Cui XM, Yuan DB, Li CY (2020) Dynamic prediction of mining-induced subsidence for any surface point based on optimized time function. Coal Sci Technol 48(10):143–149. https://doi.org/10.13199/j.cnki.cst.2020.10.018

Zuo JP, Sun YJ, Qian MG (2017) Movement mechanism and analogous hyperbola model of overlying strata with thick alluvium. J China Coal Soc 42(6):1372–1379. https://doi.org/10.13225/j.cnki.jccs.2016.1164